

The propagation, interaction and linkage of vein segments and the scatter of geometric data

Master Thesis
In Basin and Reservoir Studies

Erlend Valle Risnes



Department of Earth Science

University of Bergen

June 2019

Abstract

The lengths, widths, orientations, bridge widths and linkage characteristics of 636 vein segments from 84 arrays have been measured and analysed. The relationships between the parameters are assessed. The veins are in the Blue Lias Formation exposed on the Somerset coast, UK. E-W orientated arrays (mostly related to basin extension) are compared with N-S orientated arrays (related to later basin contraction).

The parameters measured mostly show weak correlations coefficients. Scatter in the data result both from the way vein segments propagate, interact and link and from the way measurements were made. Veins appear to propagate in three stage cycles. Stage 1: propagation, with length and width increasing proportionally. Stage 2: interaction, where a segment interacts with one or more adjacent segments, so propagation is hindered but dilation continues. Stage 3: linkage, where adjacent segments connect to form a composite segment, so length increases but maximum width does not change. These stages can be repeated for the composite segment, creating a cycle of development and segmentation across a range of scales. A steplike trajectory occurs on a plot of vein length to width. The segmentation across a range of scales means that the definition of segments can be subjective, with the number of vein segments defined being controlled by resolution. In this study, linkage was characterised in terms of topology, i.e. if a segment is not connected in the plane of view, or whether it is connected at one or both ends of the trace. This may not have been the best way to characterise the segmentation of interacting and linked vein segments.

Acknowledgements

First and foremost, I want to express my gratitude towards my supervisor David Peacock, and my co-supervisor Atle Rotevatn both from the University of Bergen. I especially want to thank David for his patience when explaining concepts of both geology and scientific writing. Further, I am grateful for financial support for fieldwork provided by the ANIGMA project from the Research Council of Norway (project no. 244129/E20), and from Statoil ASA through the Akademia agreement.

I also want to thank my field associate Erlend Gjørund for a productive fieldwork cooperation. A special thanks to the geophysicists at “Gneis” study-hall for their help with MatLab. Further, I want to thank my fellow geology students for a great study environment, especially the company of “Team Bergen”. Lastly, I want to express my gratitude towards my family for supporting me through stressful times.

Table of contents

1 Introduction	1
2 Background	3
2.1 Geological setting	3
2.2 Theoretical background	6
2.2.1 Parameters	8
2.2.2 Relationships	9
2.2.3 Ambiguities.....	10
2.2.4 Propagation, interaction and linkage.....	11
3 Methods	15
3.1 Parameters measured	15
3.2 Relationships	18
3.3 Ambiguities in the measurements.....	18
3.4 Propagation, interaction and linkage	21
4 Results	22
4.1 Parameters	22
4.2 Relationships	27
4.3 Ambiguities in the statistics.....	32
4.4 Propagation, interaction and linkage	33
5 Interpretation.....	36
5.1 The effects of vein propagation, interaction and linkage on data scatter	36
5.2 Problems with the measurements	40
6 Discussion.....	44
6.1 What is a segment?	44
6.2 Comparison with faults.....	46
7 Conclusions	50
8 References.....	51

1 Introduction

The aim of this thesis is to measure and analyse the relationship between various geometric parameters of vein arrays and discuss the significance of the data for how the veins develop. The thesis is intended as an expansion to the work of Sanderson and Peacock (2019), where they developed a systematic way of measuring and characterising the kinematics of vein arrays. Such studies can help give a better understanding of how veins develop. In contrast to the work of Sanderson and Peacock (2019) this thesis made all the measurements in situ. Additionally, this thesis adds parameters such as bridge width and bed thickness to the dataset. The data includes both topological and geometrical values of 636 veins segments from 84 arrays, all collected through photographs taken in the field. These values are supplemented with qualitative observations from the fieldwork.

The study area is in the southern margin of the Bristol Channel Basin, which is chosen because of well-exposed vein arrays. More specifically the data is collected in an area between east of Lilstock and the Blue Ben fault (Figure 1.1). The arrays are found in Limestone beds within the Blue Lias formation, which is of early Jurassic age (Procter & Sanderson, 2018). The field location has two dominant orientations for vein arrays, which is east-west (E-W) and north-south (N-S). The measurements are therefore divided into two datasets depending on their orientation. The orientations can, therefore, be compared in the results. The veins are orthogonal to the bedding plane in all cases and can, therefore, be analysed in two-dimensions. The data were evaluated through scatterplots with a linear regression analysis.

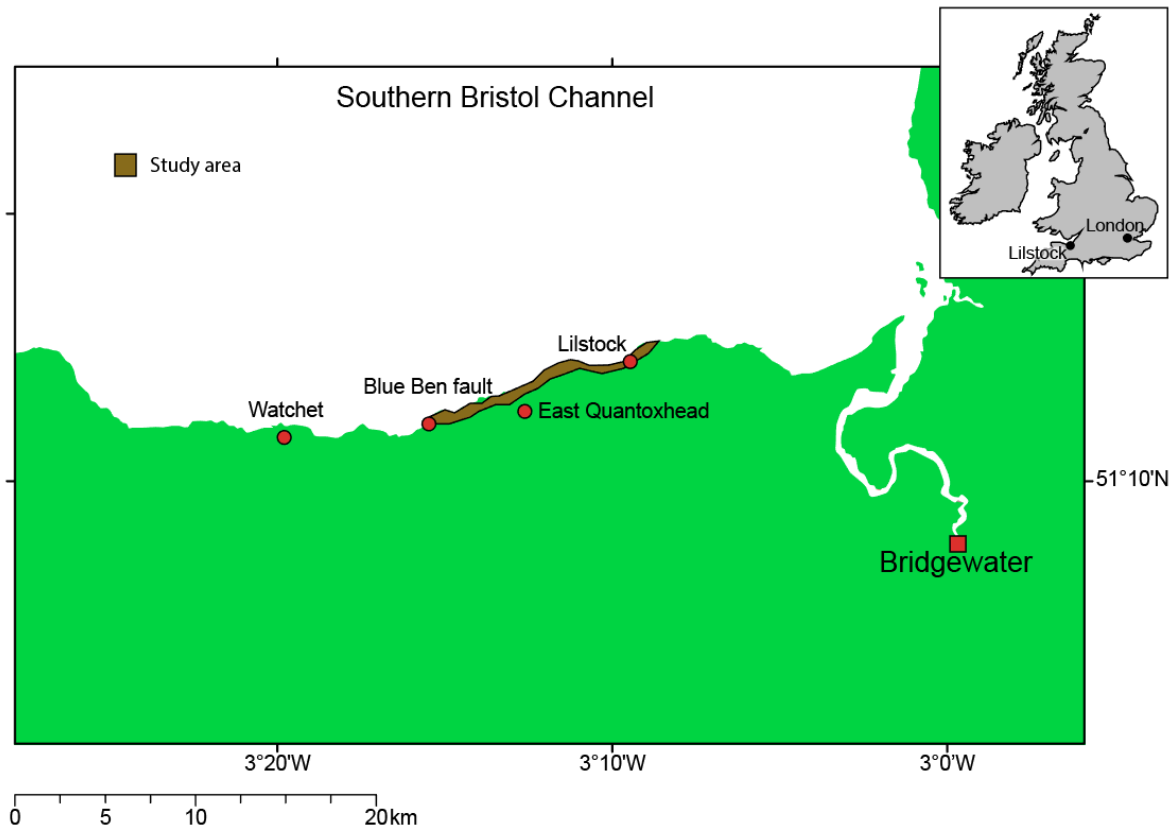


Figure 1.1 Geographical map of the Southern Bristol Channel showing the location of the study area. The map is modified from Peacock et al. (2017).

2 Background

The background chapter is divided into the two sub-chapters 2.1 Geological setting and 2.2 Theoretical background. Chapter 2.1 gives a brief introduction to the geology in the field area. Chapter 2.2 then presents the theoretical background information relevant for this thesis.

2.1 Geological setting

The study area is in the southern margin of the Bristol Channel. All the data were collected on the beach between east of Lilstock and Blue Ben fault, thus only from Liassic age (Figure 2.1). The beach is located within a basin that initiated in the Triassic, but the main extensional faulting occurred in early Cretaceous (Peacock & Sanderson, 1999). Extension caused well-developed fault systems that link through relay ramps (Peacock & Sanderson, 1991a). A Relay ramp is a zone of kinematic linkage between overlapping faults, where the strain is relayed from one fault to another (Peacock et al., 2016). Most of the E-W orientated vein arrays have developed in association to these fault systems (Peacock & Sanderson, 1991a). The basin was then inverted in the Eocene and Oligocene induced by the Alpine orogeny (Procter & Sanderson, 2018). The N-S inversion caused reactivation of the normal faults and developed cross-cutting strike-slip faults (Dart et al., 1995; Peacock & Sanderson, 1999). Most of the N-S orientated vein arrays have developed in association to these strike-slip faults (Peacock & Sanderson, 1999). The inversion also includes reverse reactivated normal faults with hanging wall buttress anticlines (Engelder & Peacock, 2001). Peacock and Sanderson (1999) suggest that the deformation history at Lilstock is more complex, where 150° extension caused 060° striking joints, veins and faults. Further, an approximate N-S extension on 095° striking faults, with sinistral transtension. Thereafter, an E-W contraction accompanied by sinistral shear on some of the 095° striking normal faults. Then dextral reactivation on some of the 095° striking normal faults. Finally, N-S contraction caused thrust and strike-slip faults, with reverse reactivation of the largest 095° striking normal faults. The majority of the joints date after the evolution of faults (Peacock & Sanderson, 1991a).

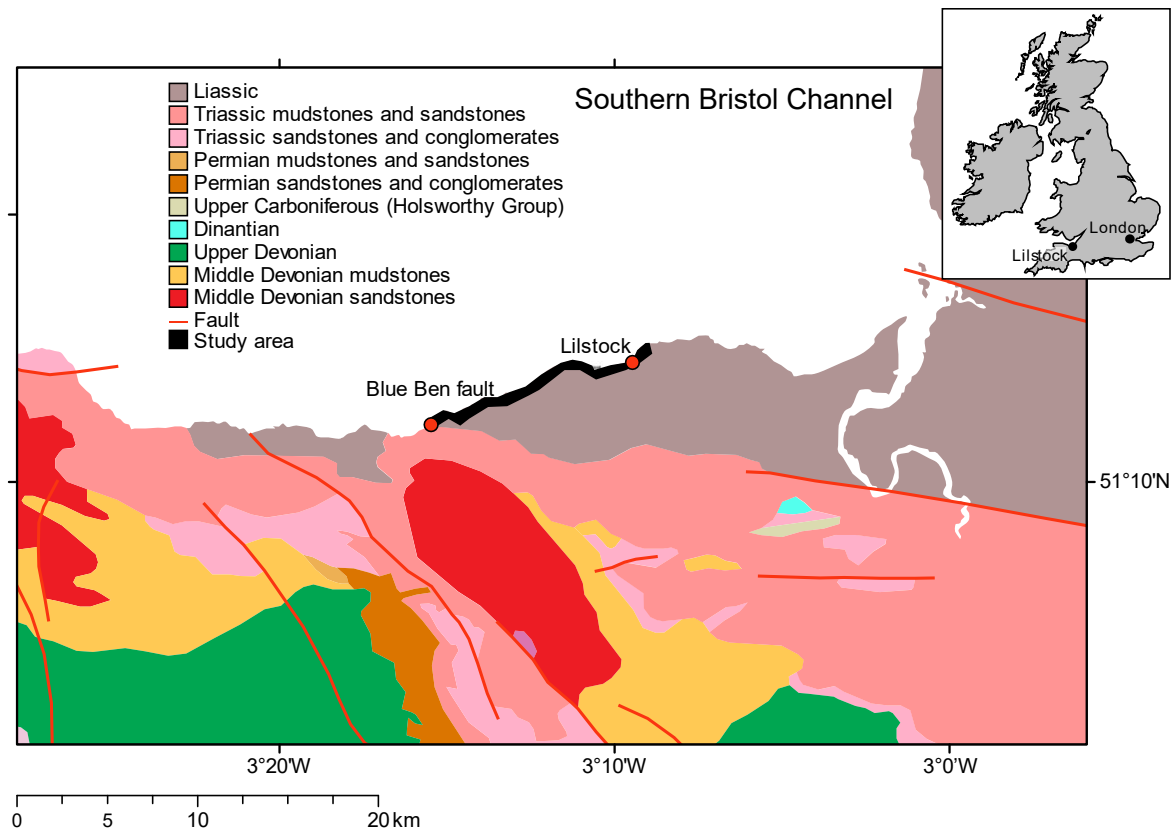


Figure 2.1 Location map of the Somerset coast, where the field area is between east of Lilstock and the Blue Ben fault. Modified from Peacock et al. (2017). The geology is from the British Geological Survey 1:625,000 scale map of the United Kingdom*.

Reproduced with the permission of the British Geological Survey ©NERC. All rights Reserved.*

The joints abut the latest fault but are not displaced by them, meaning they date post main Alpine contraction (Rawnsley et al., 1998). Both faults and veins are extensively filled with calcite but not the joints, which is a strong indication of joints being younger than veins and faults (Procter & Sanderson, 2018). The calcite fillings are due to fluid flow precipitations. If the joints were developed at the time of fluid flow, it would be reasonable to believe that the precipitation would occur in the joints as well (Procter & Sanderson, 2018). Veins and faults most likely developed in relation, whereas the joints formed during decline of Alpine compression (Rawnsley et al., 1998).

The Bristol Channel Basin is located in the northern part of the Hercynian fold belt and is filled with Triassic redbeds to Jurassic marine sediments (Van Hoorn, 1987). The field area has exposures of an interbedded sequence of shale-marl-limestone from early Jurassic known as the Blue Lias formation. Sheppard et al. (2006) concluded that the sediments in

the Blue Lias formation were originally deposited by storm activity as a homogenous bed of lime-mud. The bed was thereafter differentiated by diagenesis into an alteration between limestone and shale (Sheppard et al., 2006). Sheppard et al. (2006) therefore classify the sequence as a pseudo-bedding.

2.2 Theoretical background

Veins are extension fractures filled with a precipitated mineral (Peacock et al., 2016). The most common minerals that fill the veins are calcite, anhydrite and gypsum (Bons et al., 2012). Veins typically form an en echelon pattern (Peacock, 2004). This type of pattern is a stepped arrangement where the individual elements appear roughly parallel to each other, although they occur obliquely to the linear zone they form within (Figure 2.2; Biddle & Christie-Blick, 1985). The pattern can be observed in veins, joints, shear fractures and dykes (Peacock et al., 2016). Where Shear fractures (faults) typically form an en echelon pattern before linkage. Dykes, veins and joint are all extensional fractures. Dykes are filled with magma intrusion, whereas joints are unfilled extension fractures (Peacock et al., 2016). Although veins, joints and dykes are all extension fractures Peacock (2001) emphasize the importance of treating them separately, because they commonly form at different times under different conditions. In this thesis, however, only veins are included.

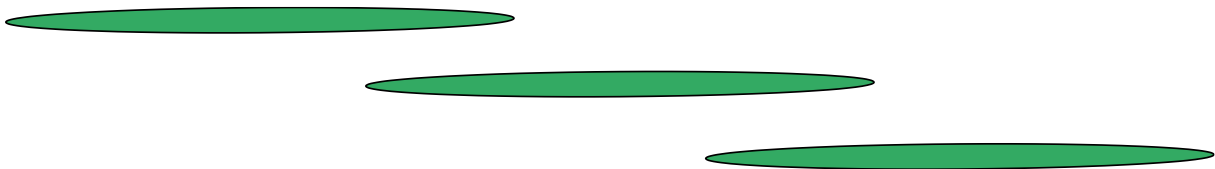


Figure 2.2 Schematic illustration of an en echelon pattern for fractures. Modified from Biddle and Christie-Blick (1985).

En echelon structures occur at scales ranging from centimetres to kilometres (Nicholson & Pollard, 1985), although the dataset only covers from a centimetre scale to approximately 6 metres. There are 18 arrays in the dataset that have developed pull-aparts. These structures are developed by extension between two overstepping faults and often occur in an array along an en echelon series (Peacock & Sanderson, 1995).

Pollard and Aydin (1988) divide fractures into three end members of failure mode (Figure 2.3). Mode I is when the displacement vector is perpendicular to the fracture plane, which includes veins, dykes, joints and fissures. Mode II is when the displacement vector is both parallel to the propagation direction and the fracture plane. Mode III is when the displacement vector is parallel to the propagation direction and perpendicular to the fracture plane (Pollard & Aydin, 1988). Both mode II and mode III are describing shear

fractures. Pull-aparts in veins are therefore characterised by failure mode I then affected by either/both mode II and mode III.

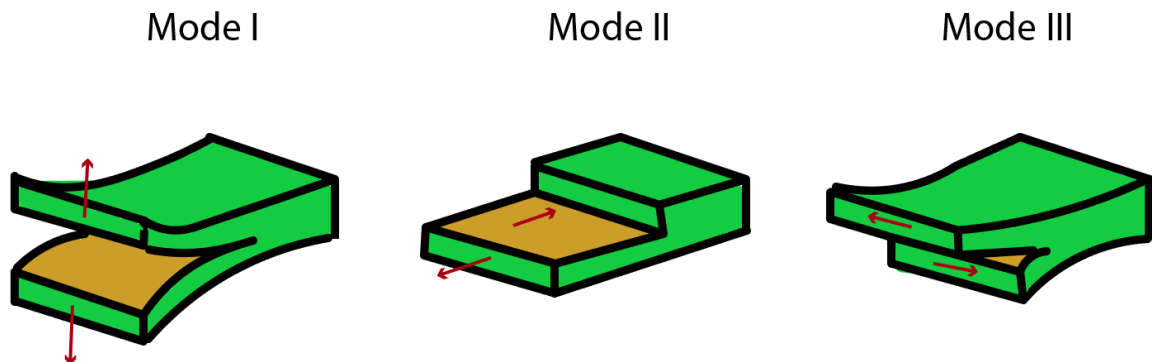


Figure 2.3 Schematic illustration of the three different end members of failure mode described by Pollard and Aydin (1988). Mode I has a displacement vector that is perpendicular to the fracture plane. Mode II has a displacement vector that is both parallel to the propagation direction and the fracture plane. Mode III has a displacement vector that is parallel to the propagation direction and perpendicular to the fracture plane. The illustration is modified from Pollard and Aydin (1988).

The rest of this chapter provides a more detailed background information on vein arrays. Section 2.2.1 presents theory on different geometrical parameters in en echelon structures. Section 2.2.2 then outlines the published scaling relationship of veins. Published scaling relationship for faults is then presented for later comparison (Section 6.1). Thereafter, Section 2.2.3 briefly presents known problems for fracture scaling analysis. Lastly, Section 2.2.4 demonstrates published models for how veins propagate, interact and link. Section 2.2.4 then presents published models for how faults propagate, interact and link for later comparison (Section 6.1).

2.2.1 Parameters

To assign geometric values to en echelon veins it is useful to divide them into segments. Peacock et al. (2016) define a segment as “an Individual fracture plane that is part of a set of subparallel fractures that forms a fracture zone”. From this, parameters such as length and maximum width can be measured for each segment. The vein segments can be linked through different structures such as stylolites (pressure solution seams), extension fractures, faults or veins (Peacock et al., 2016). When a zone is extensional en echelon veins link through extension fractures, whereas fracture systems with a high simple shear component veins tend to link through shear fractures (Peacock & Sanderson, 1995). Linkage through stylolites becomes more frequent with a higher component of transpression, until the fracture system is mainly pressure solution with no veining (Peacock & Sanderson, 1995).

McCoss (1986) developed a method for finding the infinitesimal displacement direction, which is applicable for en echelon cracks (Peacock & Sanderson, 1995). The method first draws a boundary to the array intersecting with the tips of the segments. Then draws a circle outside the zone creating a tangent at the boundary (point x, figure 2.4). Draw then a line that goes from point x parallel with the veins, in the zone, until it intersects with the edge of the circle (point y, Figure 2.4). The angle between this line and the array boundary is ω . Lastly, a line must be drawn from point y through the centre of the circle till it intersect with the edge at the other side (point z, Figure 2.4). The line that goes from point y to point z is the infinitesimal displacement direction (Peacock & Sanderson, 1995). When neglecting rotation and strain the given relationship exists:

$$A = 180^\circ - 2\omega \quad (2.1)$$

where A is the infinitesimal displacement direction and ω is the angle between the array boundary and the vein segments.

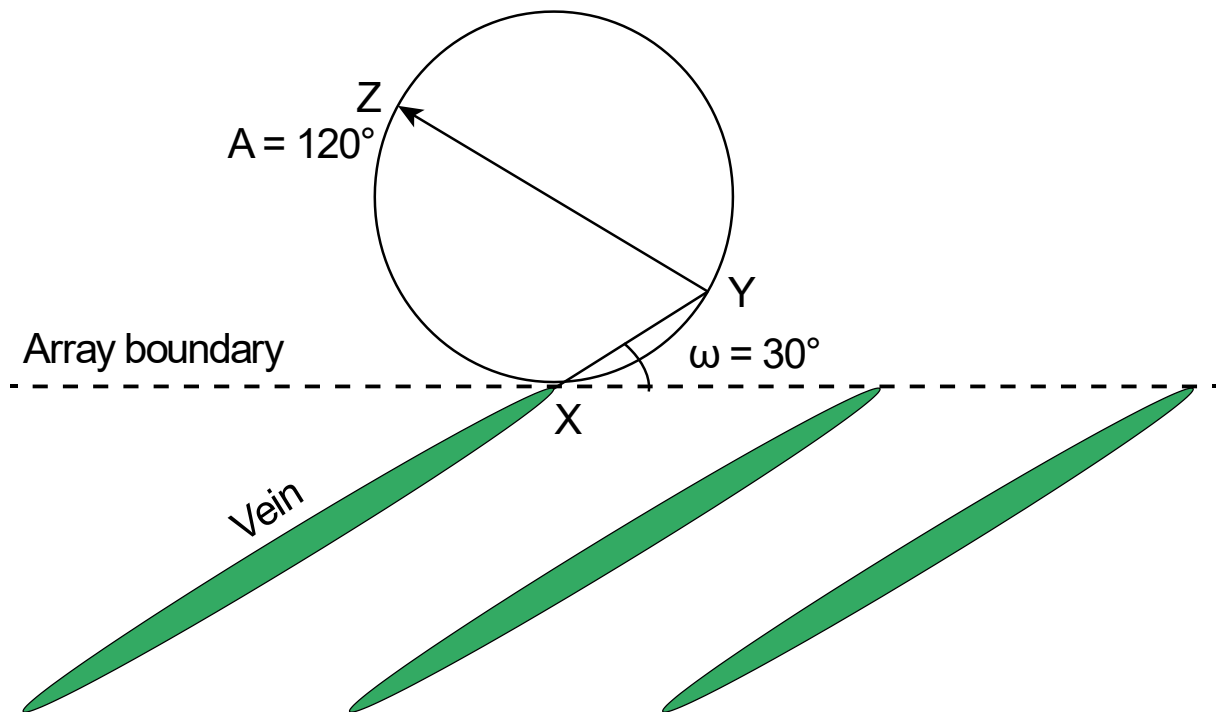


Figure 2.4 Illustration of the method for finding the infinitesimal displacement direction derived from McCoss (1986). First, the array zone boundary is drawn intersection with the vein segment tips. Then a tangent is created by drawing a circle intersecting with the array boundary at point X. Thereafter draw a parallel line from X to the edge of the circle intersecting at point Y. A line is then drawn from Y through the circle centre to the other edge intersecting at point Z. The Line from Y to Z represents the infinitesimal displacement direction. The illustration for the method is modified from Peacock and Sanderson (1995).

The spacing between two fractures that overlap is defined by Kemeny (2005) as a bridge. If the body of rock between each fracture is broken, one classifies them as a broken bridge (Schofield et al., 2012), and the two fractures become linked.

2.2.2 Relationships

The results of Vermilye and Scholz (1995) indicate a linear relationship between length and aperture for veins. Vermilye and Scholz (1995) also conclude that unconnected veins have a consistently larger aspect ratio compared to multiple-segment fractures. Olson (2003), however, argue that apertures will scale with the square root of the length for fractures that are mineralised while actively propagating. He further argues that the linear scaling relationship is restricted to cases of fracture mineralisation under relaxed unloading conditions or during the early stages of displacement driven propagations (Olson, 2003).

Fault scaling relationship is presented as maximum displacement to length (D-L). Walsh and Watterson (1988) report that there is a linear relationship between fault displacement and length. Cartwright et al. (1995), however, state that the deviation from a constant D/L ratio is due to the style of growth. When a fault segment starts to interact with an adjacent segment it will be hindered in length propagation, whilst continuing to grow in displacement. This causes a relative increase in length compared to displacement, therefore deviating from the constant D/L ratio. When the two segments connect the length is shared, thus increasing relatively to the displacement. This deviation will cause scatter in a D-L plot (Cartwright et al., 1995). Dawers and Anders (1995) state that the displacement is growing during and after linkage of two segments, which means that the aspect ratio is less affected by linkage. The constant displacement to length ratio will then persist after linkage. However, Cartwright and Mansfield (2001) report fault segments to grow individually even after linkage, and therefore cause scatter.

2.2.3 Ambiguities

Bonnet et al. (2001) state that analysis of scaling properties requires large datasets, because of a high degree of uncertainty. The scaling properties of fracture systems are often assessed through 2-dimensional parameters, and therefore ignoring 3-dimensional features in a fracture. The measurements are therefore reliant on extrapolation causing ambiguities in a relationship plot.

2.2.4 Propagation, interaction and linkage

Peacock (1991) suggests three stages of development of vein segments. Stage 1 includes isolated vein segments that do not interact with adjacent segments. These veins propagate in a constant aspect ratio. Stage 2 is when the veins start to interact, causing a decrease in the rate of length development, although the dilation is unhindered. Stage 3 is when the vein connects, which makes the two segments share length, thereby increasing the length relative to the maximum width.

Nicholson and Pollard (1985) arrange en echelon cracks into a spectrum based on the geometric form of their propagation paths. The two end members of this categorisation are distinguished as having either straight or highly curved propagation paths. In the straight propagation path, the bridges bend in order to accommodate dilation (Figure 2.5.a), whereas in the curved propagation path the bridges rotate in order to accommodate dilation (Figure 2.5.b). The curvature of the propagation path comes from interactions between adjacent crack tips (Pollard et al., 1982). The stress field around the one crack tip alters the stress field at the next increment of crack growth, so it is not parallel to the prior increment (Nicholson & Pollard, 1985). The geometrical differences between the two end members are mainly affecting the tips of the vein segment (the linking part). Both end members increase in dilation drastically after bridge failure (Nicholson & Pollard, 1985). The outer parts of the vein segments are not affected by the sudden increase in dilation to the same degree, which promotes the growth of a tail to each segment.

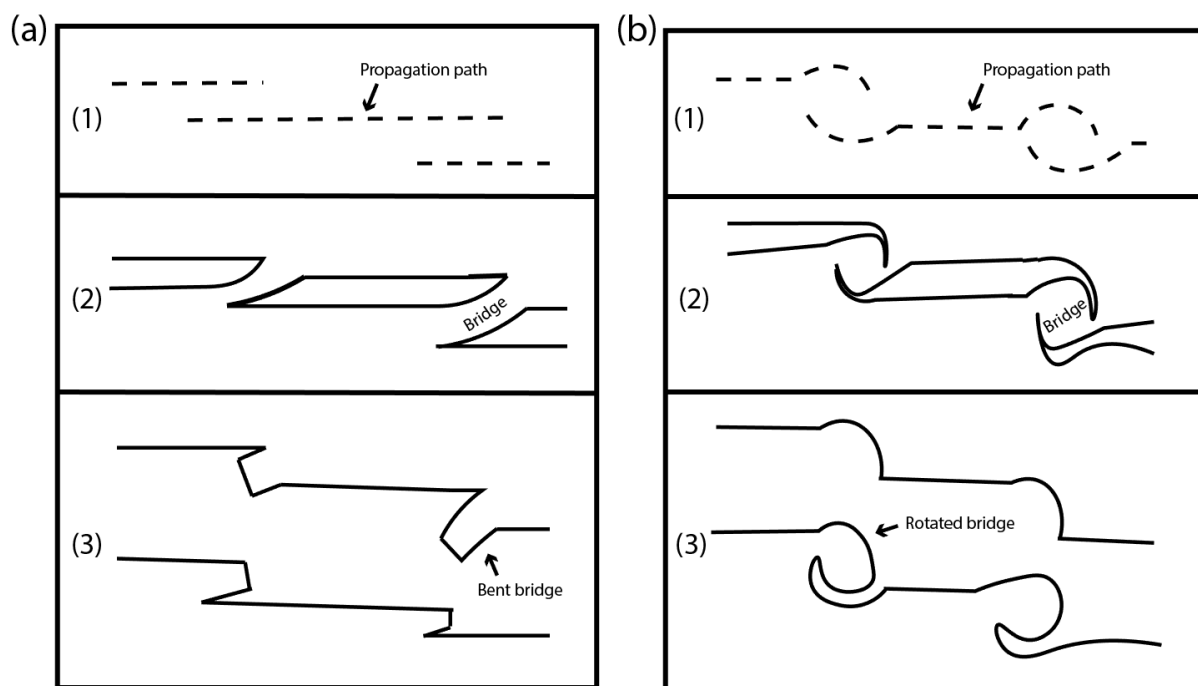


Figure 2.5 (a) Illustration of a straight propagation path where the bridges bend in order to accommodate dilation. (b) Schematic figure demonstrating how a curved propagation path is rotating the bridges in order to accommodate dilation. The illustration is modified from Nicholson and Pollard (1985).

Olson and Pollard (1991) suggested a model for the development of an echelon fracture system. Firstly, the fractures initiate with randomly oriented grain-scale flaws in the rock (Figure 2.6.a). Further, the flaws grow into microcracks and adjust perpendicular to the least compressive stress axis (Figure 2.6.b). When the cracks become long enough relative to their separation they start to interact. This favours the growth of an echelon pattern (Figure 2.6.c). If the vein configuration is exposed to more subsequent deformation it will develop localised shearing in the en echelon structures (Figure 2.6.d; Olson & Pollard, 1991).

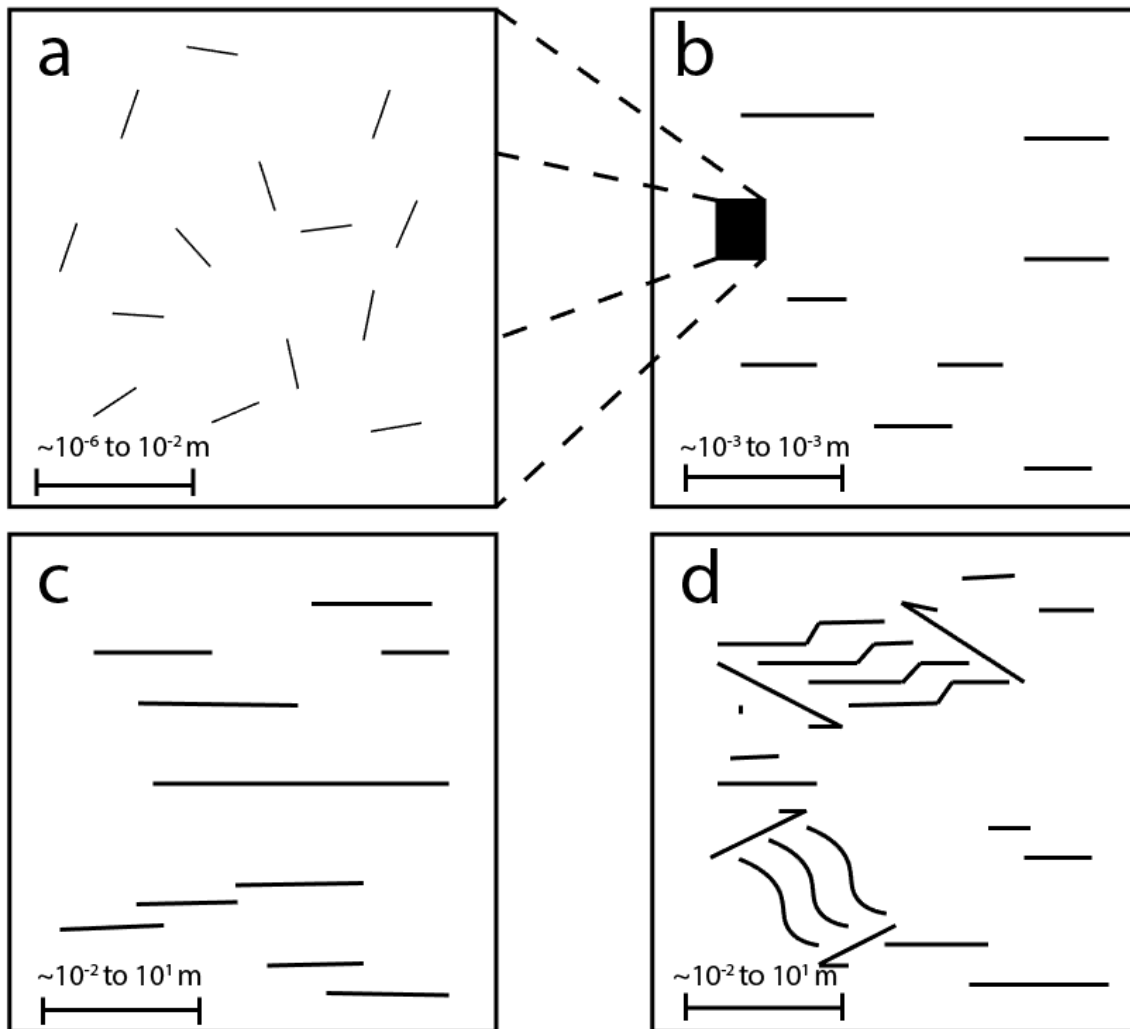


Figure 2.6 (a) Micro flaws initiate randomly in the body of rock. (b) Thereafter the flaws adjust perpendicular to the least compressive stress axis. (c) The cracks start to interact with adjacent segments favouring an en echelon pattern. (d) Localised shearing can develop from more subsequent deformation. The illustration is modified from Olson and Pollard (1991).

Beach (1975) distinguishes between en echelon veins developed during deformation and en echelon that develop into shear zones. Beach (1975) categories the en echelon fractures further into two subcategories sigmoidal and non-sigmoidal shape. The sigmoidal vein segments are formed by progressive simple shear with active pressure solution present, whilst non-sigmoidal vein segments dilate perpendicular to the length (tensile). If the non-sigmoidal vein segments undergo shear deformation they start to kink and then pull apart, displaying itself as a parallelogram (Beach, 1975). The sigmoidal shape vein segments are easily confused with pull-aparts with wing-cracks. Wing-cracks or Tail cracks are extension fractures developed at the tips of shear fractures (Peacock et al., 2016).

Sanderson and Peacock (1991a) proposed a model for how fault zones develop through propagation, interaction and linkage of segments. Sanderson and Peacock (1991a) identified a four-staged development of propagation, interaction and linkage for faults. Stage 1 is the growth of faults with no overlapping nor interaction with adjacent faults. In stage 2 overlap develops, which causes displacement transfer through a relay ramp. The difference in displacement is at its maximum at each tip of the interacting faults. Stage 3 occurs when the relay ramp begins to break down through minor antithetic faults starting to connect the two segments. Antithetic faults are associated with bending at relay ramps, which connects the bigger synthetic faults. Antithetic faults have an opposite sense of shear to a related dominant fault (Gibbs, 1984; Peacock et al., 2016). Stage 4, in Sanderson and Peacock's model (1991), is when a fault cuts off the ramp fully connecting the two segments. The linkage ends up looking like a normal drag, and the displacement is decreased in the area of linkage. The wide range of scales presented in different scientific writing suggests that linkage appears regardless of scale (Dawers & Anders, 1995; Peacock & Sanderson, 1991a; Scholz et al., 1993).

3 Methods

The methodology chapter provides insight into how the data was collected all from field observations to picture analysis (Section 3.1). Thereafter, a brief description of the statistical analyses done to visualize the relationships between the parameters (Section 3.2). Section 3.3 is a thorough review on how there are ambiguities in the measurements. Lastly, Section 3.4 describes how qualitative data have been collected, through field observations and analysis of photographs.

3.1 Parameters measured

The data were collected by measuring photographs taken during fieldwork. Photographs were taken perpendicular to bedding planes to reduce image distortion. A measurement tape was placed parallel to each vein array to act as a scale. Each array was recorded by taking several photographs along their length, and these were merged (with Adobe Photoshop) to display the full array. Vein parameters were measured on these image merges. Sanderson and Peacock (2019) show data for various vein parameters, but that work is expanded here and includes the following (Figure 3.1):

- 1) Vein segment length (L): the distance between each tip in a vein.
- 2) Maximum width (W): the maximum width of a vein, measured perpendicular to the length.
- 3) Angle (θ) of a vein segment to the boundary of the vein array.
- 4) Linkage: the number of vein segments each vein segment connects to: 0,1,2.
- 5) Bridge width (BW): minimum spacing between each vein segment.
- 6) Bed thickness: the thickness of the bed in which the vein array is located.

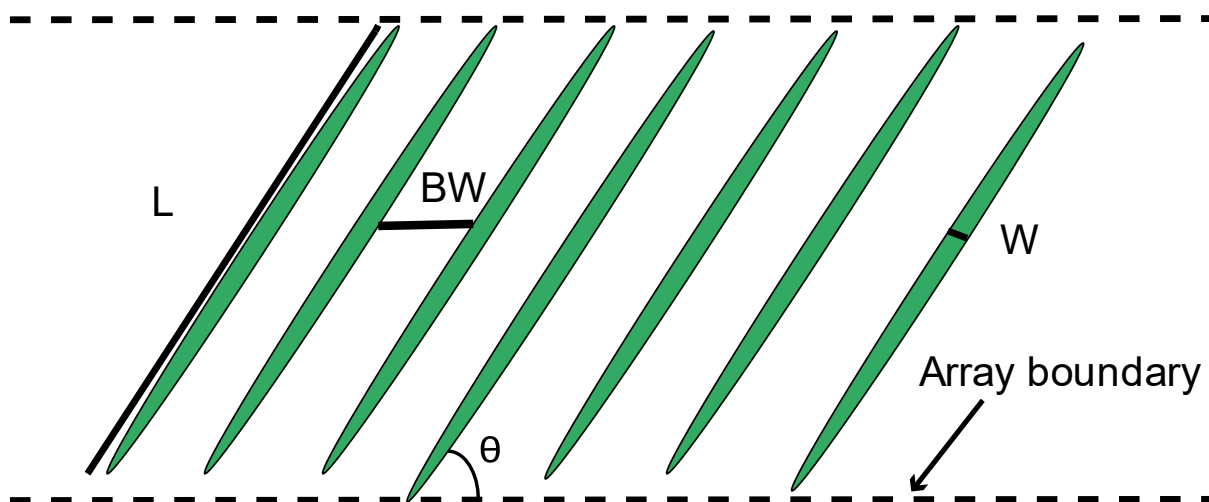


Figure 3.1 Illustration of five of the parameters measured. L is the length of a vein segment, BW is the width of the bridge, θ is the angle of the vein segment and W is the maximum width of the vein segment.

These measurements are sorted into two categories, based on their orientations and relationships to different fault types. 49 arrays ~ E-W arrays associated with normal faults were measured, and 35 ~ N-S arrays associated with strike-slip faults were measured. The structural association for each array was determined by field observations. Strike measurements were taken, with a standard geology compass, to supplement the field observations. The data consist of 433 ~ E-W vein segments and 203 ~ N-S vein segments. These measurements were all made from rocks that are in situ. Note that the measurements are all limited to two dimensions. The rest of this Section is a review on the methods used for measuring each parameter.

All distance measurements from the photographs were made using the “segmented line tool” in ImageJ software. ImageJ is an open platform for scientific image analysis, that makes it easy to modify the scale based on the scanline. A line is drawn and set as the indicated length of the measuring tape. The length of a vein segment was measured as a straight line from tip to tip (Figure 3.1). The maximum width of the vein segment is measured from the vein segment boundary on each side, perpendicular to the vein segment length (Figure 3.1). The length of a vein segment and the maximum width of that vein segment is used to compute the aspect ratio (L/W).

The method for measuring the angle of a vein segment within an array is derived from Sanderson and Peacock (2019), which is the angle of the vein segment from the array

boundary. In order to measure this angle, a hypothetical line needs to be drawn (array boundary) along the vein segment tips (Figure 3.1). The intersection point between the array boundary and the vein segments constructs the vertex of the angle, and thus forms the angle between each line. The array boundary is drawn as a straight line through the whole array, similar to the method derived by McCoss (1986). Θ is therefore equal to ω (see Section 2.2.1). The angle is an implication of the degree of overlap between two vein segments. This is demonstrated by Beach (1975) as the ratio between overlap and length (length of overlapping area/ length of the segment) displays a linear relationship to the angle of the vein segment. The angle was measured with the angle tool in ImageJ.

The degree of vein segment linkage is recorded as an integer from zero (neither tips connected to an adjacent vein segment) to two (both tips are connected to adjacent vein segments). For example, the linkage is “one” if the vein segment is linked at one tip but not at the other tip (Figure 3.2). If the array dies out with one segment that is connected at the other end, it is recorded as linkage = 1. The segments are predominantly connected through veins, but a significant amount have developed as pull-aparts, thus connecting through faults. This parameter is not controlled by the thickness of the linkage, which means that the degree of the bridge breach does not affect the value. The parameter is also limited to two dimensions, thus neglecting linkage that is not visible on the bedding plane.

(a) 0-linkage



(b) 1-linkage



(c) 2-linkage



Figure 3.2 A schematic figure of the different degrees of linkage. (a) Neither the tips are linked with an adjacent vein. (b) The vein is connected to another segment only at one tip. (c) The vein segment is connected to adjacent veins at both tips.

The bridge width is determined as the minimum distance between two vein segments, which are overlapping each other (Figure 3.1). When the bridge is breached the two segments become linked. The thickness of the limestone beds was measured at the location with a standard measurement tape, identical to the one used for scanlines.

3.2 Relationships

To visualise the relationships between the parameters several scatter plots have been made. The data were imported to MatLab, and then plotted against each other to display correlations. A linear regression analysis was made to identify the general trend for the scatter plot. The method of regression is the least-squares regression analysis. This method finds the least-square distance from a point to a function, which means that it iteratively draws a square for each point where the length of the sides is equal to the vertical distance to the function (Haenlein & Kaplan, 2004). The correlation coefficients for each regression line is defined as the covariance between two variables divided by the standard deviation of both variables squared (equation 3.1), (Lawrence, 1989).

$$\rho_{x,y} = \left(\frac{cov(X,Y)}{\sigma_x \sigma_y} \right)^2 \quad (3.1)$$

where ρ is the coefficient, x and y are the two variables and σ is the standard deviation for each variable. The output is a number between -1 and 1, where -1 and 1 is perfect correlation and 0 has no linear correlation (Lawrence, 1989).

3.3 Ambiguities in the measurements

The precision of the measurements is controlled by various conditions. Two of them are the quality of the image as well as the accuracy of the measuring tape. Each photograph has dimensions of 3872 x 2592 pixels, and a size of approximately 4.3 Mb, with resolution and pixel size being controlled by the distance between the camera and the rock surface. When looking at smaller structures the image will show pixilation, which can make it difficult to determine boundaries. The smallest division of the scale on the measuring tape is 1 mm, which provides an uncertainty of $\pm 0.5\text{mm}$. Further variables that affect the precision of the

measurements can be individual eyesight, camera lens distortion, software uncertainties and distortions from photo merging in Adobe Photoshop.

The length of a vein segment was measured as a straight line. This means that vein length will often be underestimated because veins can be kinked or curved, thus their true length is an aggregation of several length measurements. Additionally, vein segments commonly interact and link with each other such that it is difficult to tell where one begins and the other ends. Several vein segments splay at their tips, which also makes it difficult to identify their tips. Furthermore, vein segment widths decrease from the location of maximum width to zero at the vein segment tips, making it difficult to accurately locate the end point. These faint tips are even harder to locate in an image with a finite number of pixels.

There are fewer problems to consider when measuring the width of a vein segment than that of length. Nonetheless, the uncertainty involved is bigger than length measurements in terms of percentage. Suppose a vein segment has a length of 20.00 cm and a width of 1.00 cm, where the errors of measurements are 1.00 cm and 0.20 cm, respectively. The uncertainty involved would be 5.0 % for length and 20.0 % for width. The measuring tape has an uncertainty of ± 0.05 cm (see Section 3.1) and the thinnest vein was measured as 0.02 cm, which gives an uncertainty higher than the measured value (i.e. ~ 250 %). Measuring width is especially difficult for narrow veins, with the % error being higher than for wider veins. Joints follow some vein segments, which increases the width of the vein. To find the true width, it is necessary to subtract the width of the joint. The true width is a result of two measurements, and therefore the uncertainty involved increases. Dissolution of the calcite can widen the joints within the vein, which makes this method of finding the “true” width ambiguous. The uncertainty associated with aspect ratio is the combined uncertainty to both width and length. The errors in the measurements of bridge width and maximum segment width are identical, as they are both distances controlled by the vein segment boundary.

The boundary of a vein array can be curved (Figure 3.3). This causes problems when measuring the angle of a segment because the method of measuring treated the array boundary as a straight line. There were also problems extrapolating the shorter vein segments to the vein array boundaries. Extrapolating inaccurately can alter the baseline of the angle, which induces an error in the angle measurement.



Figure 3.3 A curved array boundary causes problems when measuring the angle of a vein segment because the method of measurement only considers a straight array boundary.

Assigning the linkage value as an integer can be misleading, as the breach in the bridge progresses gradually. In terms of development, the difference between an unlinked and a linked array can, therefore, be next to none. At the early stages of linkage, it can also be difficult to differentiate between unlinked and linked segments. A breach in a bridge can be faint, and therefore difficult to identify on photographs.

Bed thickness varies laterally, the upper surfaces of beds can be weathered, and the transitions to underlying shales can be ambiguous, so there is some uncertainty in the measurements. The measurements are therefore rounded to the nearest half centimetre.

3.4 Propagation, interaction and linkage

The veins are further studied by observations made through photographs. The observations are restricted to how veins interact and link. It is further interpreted if the width of the vein is widened by shear displacement. The E-W veins with shear displacement have developed throw. These veins were interpreted to be small faults and were therefore excluded from the dataset.

4 Results

Section 4.1 provides statistical values of the parameters described in Section 3.1, and their relationships described in Section 4.2. It is, however, necessary, to emphasize that this thesis aims to analyse relationships between the parameters, which is why the thesis focuses on the results from Section 4.2. An explanation of how there are ambiguities in the statistics are presented in Section 4.3, followed by observations of interactions between vein segments in Section 4.4.

4.1 Parameters

All the statistical values that have been calculated for individual parameters are presented in table 4.1. The values are calculated for both E-W veins and N-S veins to illustrate possible differences and similarities.

Table 4.1 Overview of the statistical values calculated for individual parameters.

Parameter	Orientation	Mean value	Maximum value	Minimum value	Mode value	Standard deviation
Length (cm)	E-W veins	18.53	286.05	0.59	2.55	27.53
	N-S veins	19.83	202.41	0.45	1.88	24.47
Maximum Width (cm)	E-W veins	0.32	3.73	0.02	0.11	0.33
	N-S veins	0.79	7.17	0.03	0.06	1.04
Angle (°)	E-W veins	9.35	56.68	0	0	7.49
	N-S veins	16.58	78.85	0	0	13.68
Linkage	E-W veins	1.02	2	0	0	0.78
	N-S veins	0.70	2	0	0	0.86
Bridge width (cm)	E-W veins	0.68	7.26	0	0.10	0.83
	N-S veins	1.03	13.67	0	0	1.56
Bed thickness (cm)	E-W veins	25.72	45	12	25	7.58
	N-S veins	27.58	44	8	30	8.08

The length parameter behaves similarly for both orientations of veins, as the mean value is approximately the same (Table 4.1). The high standard deviation suggests a wide range of values, confirmed by 95 % of the data are within a range of 0 cm - ~70 cm. The characteristics of length data make it random which value appears most frequently, thus

making the mode inappropriate for analyses. Figure 4.1 is a normal distribution plot, which shows little differences between the two orientations. The generally higher frequency for E-W veins is due to the lower quantity of vein segments in the N-S orientated dataset.

The mean values indicate that E-W veins are on average half as wide as N-S veins (Table 4.1). Maximum width values have high dispersion for both orientations, which is demonstrated by the high standard deviations. The standard deviations imply that 95 % of the values are within a range of 0 cm – 0.98 cm for E-W veins, and 0 cm - 2.87 cm for N-S veins. The characteristics of width data make the most frequently appearing value random, comparable to length data, therefore the mode becomes inappropriate for analyses. Figure 4.2 shows a clear difference between the two orientations, reflected by the different shapes in the normalisation plot. The distribution fit for E-W veins is steep in comparison to N-S veins, indicating a narrower variation in the data.

The mean values indicate that E-W veins on average have half the angle as N-S veins (Table 4.1). Angle values have high dispersion for both orientations, demonstrated by the high standard deviations. The standard deviations imply that 95 % of the values are within a range of 0 ° – ~25 ° for E-W veins, and 0 ° - ~45° for N-S veins. The mean value, however, is higher than the standard deviation, indicating narrower dispersion than for maximum width values. Figure 4.3 shows a clear difference between the two orientations, reflected by the different shapes of normalisation plot. The distribution fit for E-W veins is steep in comparison to N-S vein, indicating a narrower variation in the data.

Linkage values tend to be slightly lower for E-W orientated veins (Table 4.1). The standard deviation is naturally low for both datasets because they are limited to three values (0,1,2). The standard deviation values are therefore 0.78 for E-W veins and 0.86 for N-S veins. Even though the mean value for both datasets is close to 1, the mode for both orientations is 0. The least common value for E-W veins is 2, and the least common value for N-S veins is 1.

The mean values indicate that E-W veins have on average thinner bridges than N-S veins (Table 4.1). Bridge width values have high dispersion for both orientations, reflected by the high standard deviations (see Table 4.1). The standard deviations imply that 95 % of the values are within a range of 0 cm – 2.34 cm for E-W veins, and 0 cm – 4.15 cm for N-S veins. The mean value is lower than the standard deviation, indicating a wide range in values.

Figure 4.4 shows clear a difference between the two orientations, demonstrated by the different shapes in the normalisation plot. The distribution fit for E-W veins is steep in comparison to N-S vein, indicating a narrower variation in the data.

The difference in bed thickness between the two datasets is marginal. Statistical values indicate that E-W veins are slightly more frequent in thinner beds (Table 4.1), which is supported by the normalisation plot (Figure 4.5). The implications of the statistical differences are presumably negligible, as the measurements were made at near random in different beds.

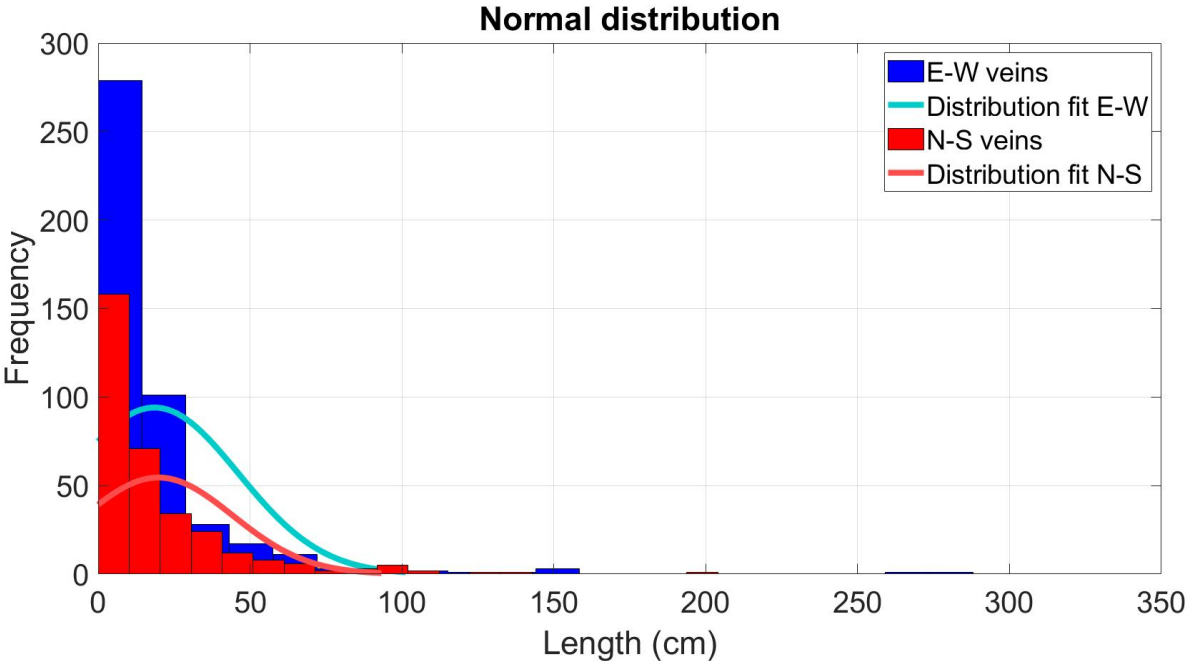


Figure 4.1 Graph showing the distribution of length values. The normal distribution curve indicates that there are marginal differences between the two vein orientations. The number of columns is set to 50 for both datasets.

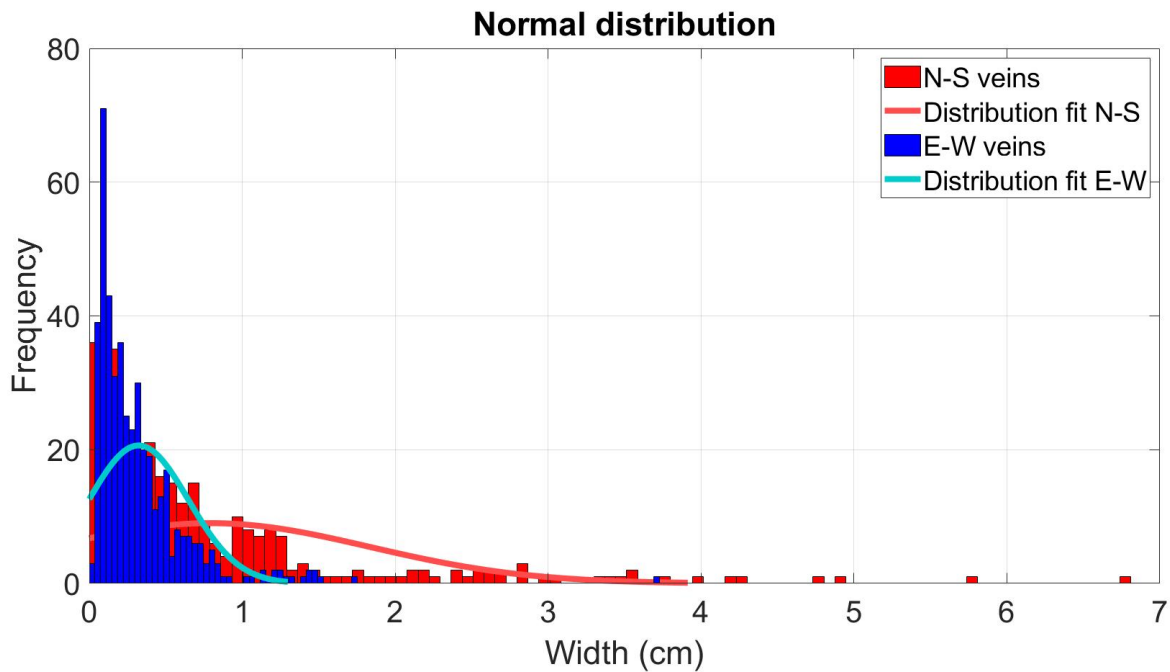


Figure 4.2 Normal distribution plot of maximum width indicates that N-S veins are generally wider than E-W veins. N-S veins have a much wider range in comparison to E-W veins, reflected by the flatter bell curve. The number of columns is equal to 100 for both datasets.

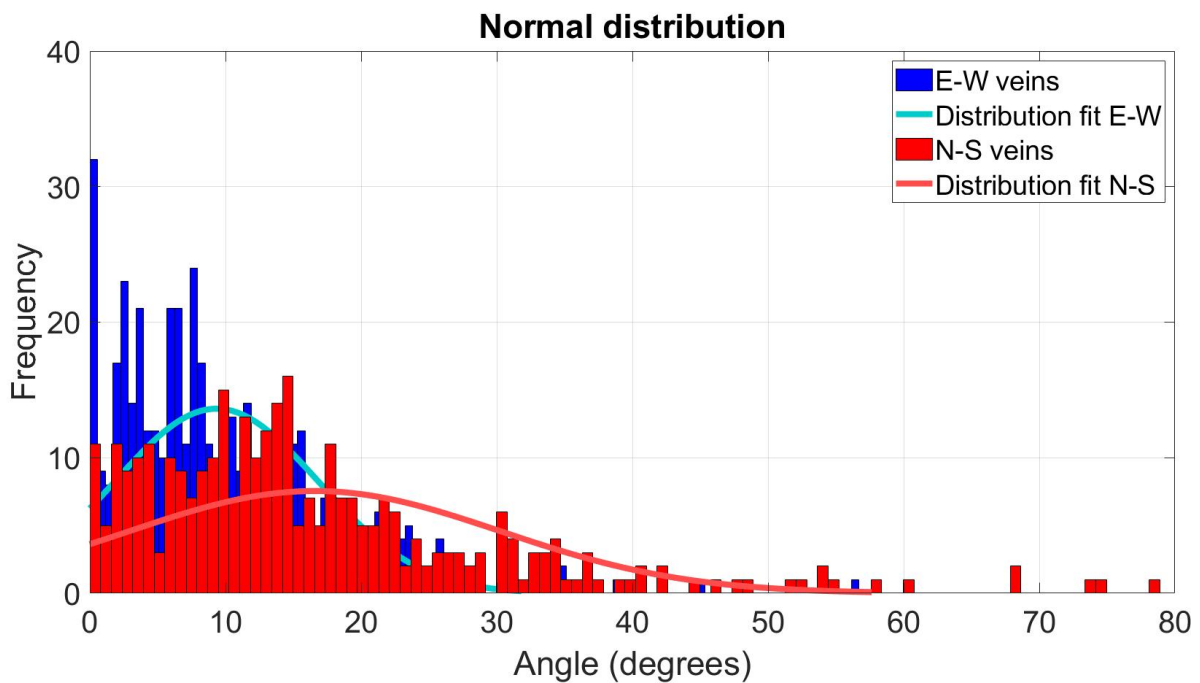


Figure 4.3 Normal distribution plot of angle showing that N-S veins cover a wider range of values. E-W veins tend to not exceed 30°, whereas N-S veins can reach over 40°. The number of columns is equal to 100 for both datasets.

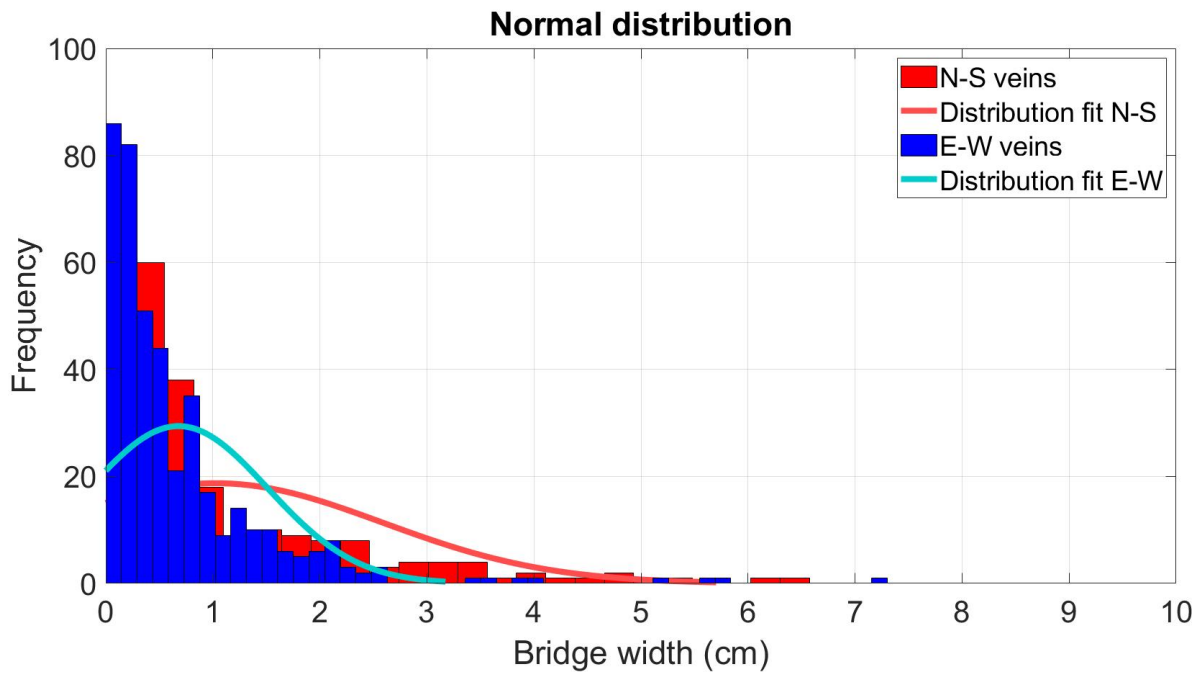


Figure 4.4 A normal distribution plot of bridge width. The range of values seems to be wider for N-S veins than E-W, although the highest value is E-W orientated. The number of columns is equal to 50 for both datasets.

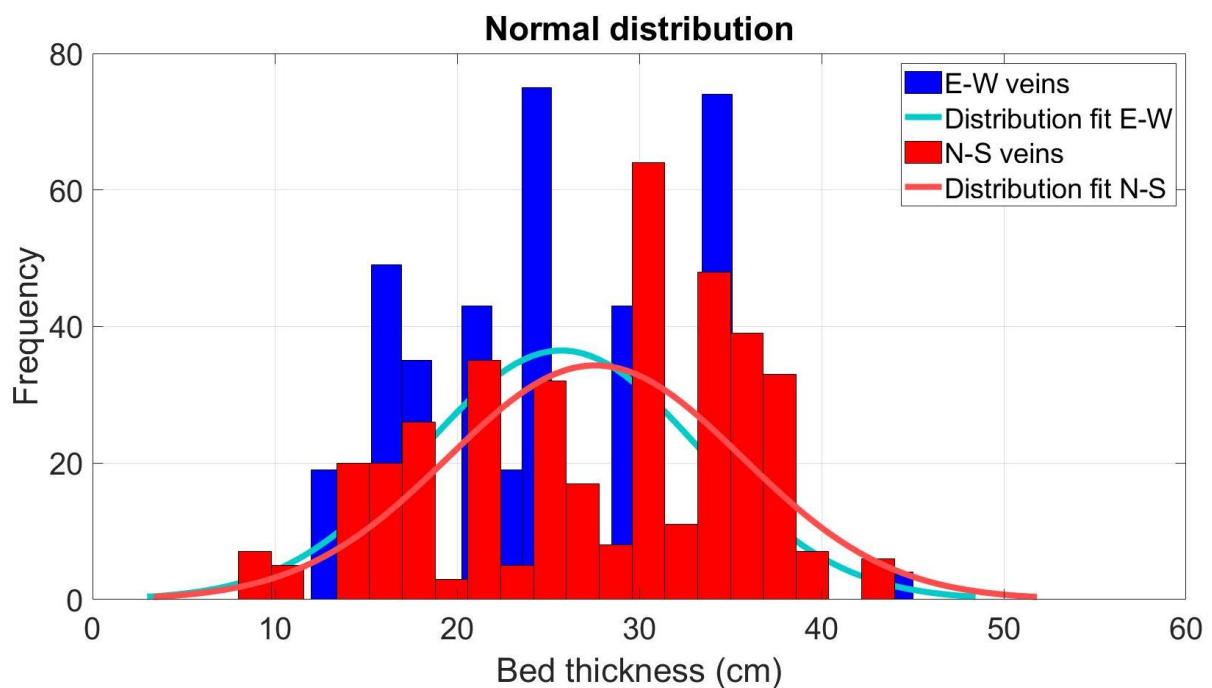


Figure 4.5 Graph illustrating the similarities in bed thickness between the two datasets. The plot indicates that E-W veins are slightly more common in thinner beds. It is, however, likely that variation between the two orientations is random. The number of columns used for both datasets is equal to 20.

4.2 Relationships

Segment length appears to increase as maximum width increases (Figure 4.6), but the linear correlation coefficients are poor with $\rho = 0.37$ for E-W orientated veins and $\rho = 0.11$ for N-S orientated veins. The coefficient for E-W orientated veins indicates a weak correlation, whereas the coefficient for N-S orientated veins implies weak to no correlation. Figure 4.6 shows that the scatter in N-S veins is larger than for E-W veins. The regressed line for N-S veins has a higher intersection point, which coincides with the higher mean value for maximum width (Table 4.1).

The mean linkage value for each array has been calculated by summing all the linkage values and dividing them by the number of segments (equation 4.1).

$$M = \frac{\sum_{i=1}^S Li}{S} \quad (4.1)$$

where M is the mean linkage, S is the number of segments and L is the linkage value for each segment. These values are plotted in Figure 4.7 against maximum width and applies to all graphs with mean linkage. In Figure 4.7 there are several data points with exact same linkage value and varying maximum width. This is because the mean linkage value applies to the whole array giving all the vein segments within the array the same value. Figure 4.7 suggests that arrays with high mean linkage tend to be wider. The correlation coefficient for E-W orientated veins is $\rho = 0.09$, whilst for N-S orientated veins it is $\rho = 0.47$. The coefficient implies that E-W veins show no correlation between mean linkage and maximum width, whereas N-S veins show some correlation to some extent.

The least-square regression method indicates a low linear relationship between length and mean linkage for both datasets (Figure 4.8). The E-W vein regression line fits poorly and has a correlation coefficient of $\rho = -0.08$. The N-S regression line, however, fits better and has a correlation coefficient of $\rho = -0.19$.

The relationship between angle and aspect ratio has a negative correlation, which is demonstrated in Figure 4.9. The y-variables are the logarithm of the aspect ratio, in order to analyse the large range of quantities. This applies for all the graphs with aspect ratios as a variable. The veins are predominantly below 45 degrees with few exceptions which

essentially are N-S orientated veins. Calculations indicate that both E-W veins and N-S veins have a coefficient of $\rho = -0.20$.

The E-W veins have a correlation coefficient between mean linkage and aspect ratio of $\rho = -0.05$. This is a very low correlation coefficient indicating a non-existing relationship. N-S veins have a higher correlation coefficient of $\rho = -0.27$. Both regression lines are presented in Figure 4.10.

The relationship between angle and mean linkage is weak for both orientations (Figure 4.11). E-W veins have a correlation coefficient of $\rho = -0.18$, whereas N-S veins have $\rho = -0.004$. The E-W veins show some linear correlation whereas the linear relationship for N-S veins is non-existing.

Bed thickness has a slight correlation with width for E-W orientated veins. The correlation coefficient for these variables was calculated to $\rho = 0.28$. In contrast, N-S vein variables were calculated to have a coefficient of $\rho = -0.028$. The least-square regression analysis that is performed on the two datasets shows a positive relationship for E-W veins and a slight negative relationship for N-S veins (Figure 4.12), which coincides with the coefficient calculations. There are many width values with identical bed thickness, which is because the bed thickness is rounded to nearest half centimetre.

All the correlation coefficients that have been calculated for the relationships between parameters are presented in table 4.2. The values are divided into E-W veins and N-S veins to illustrate possible differences and similarities.

Table 4.2 Overview of the correlation coefficient calculated for relationships between parameters.

Orientation	Correlation coefficient (ρ)	
	E-W veins	N-S veins
Length to maximum width	0.37	0.11
Maximum width to mean linkage	0.09	0.47
Length to mean linkage	-0.08	-0.19
Angle to log (Aspect ratio)	-0.20	0.20
Aspect ratio to mean linkage	-0.05	-0.27
Angle to mean linkage to	-0.18	-0.004
Bed thickness to maximum width	0.28	0.08

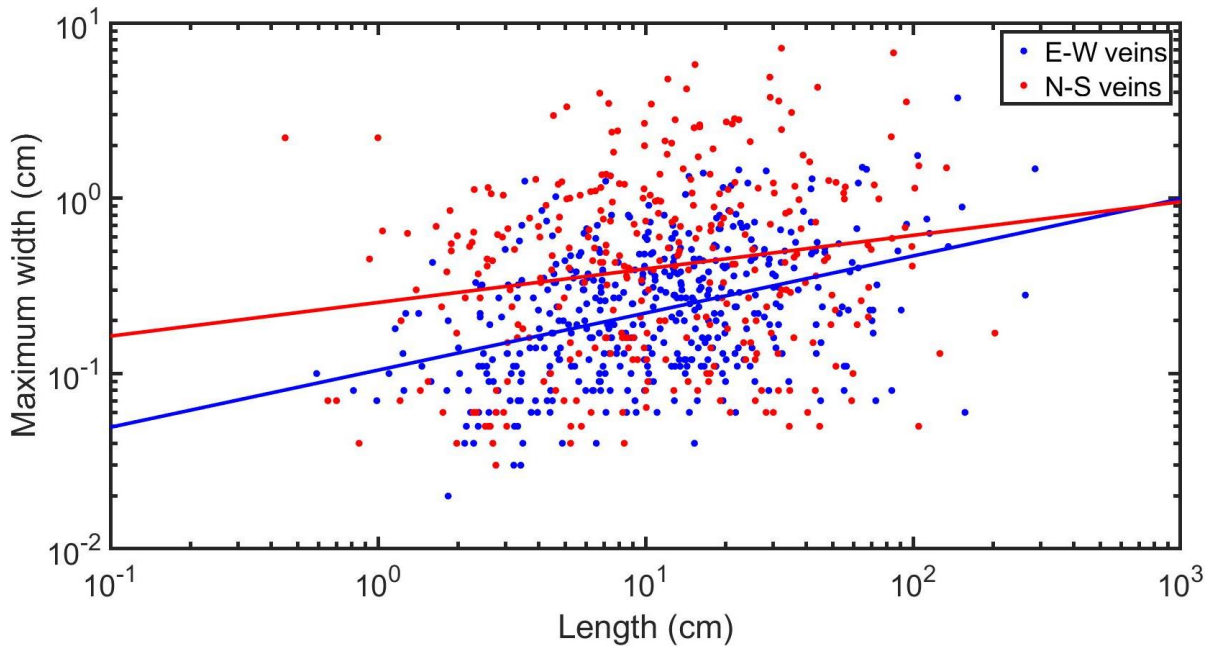


Figure 4.6 Graph showing length of vein segments against maximum widths. The E-W veins demonstrate a moderate correlation with a coefficient of $\rho = 0.37$, whereas N-S veins indicate a weaker relationship with a coefficient of $\rho = 0.11$. Note that both axes are in logarithmic scale.

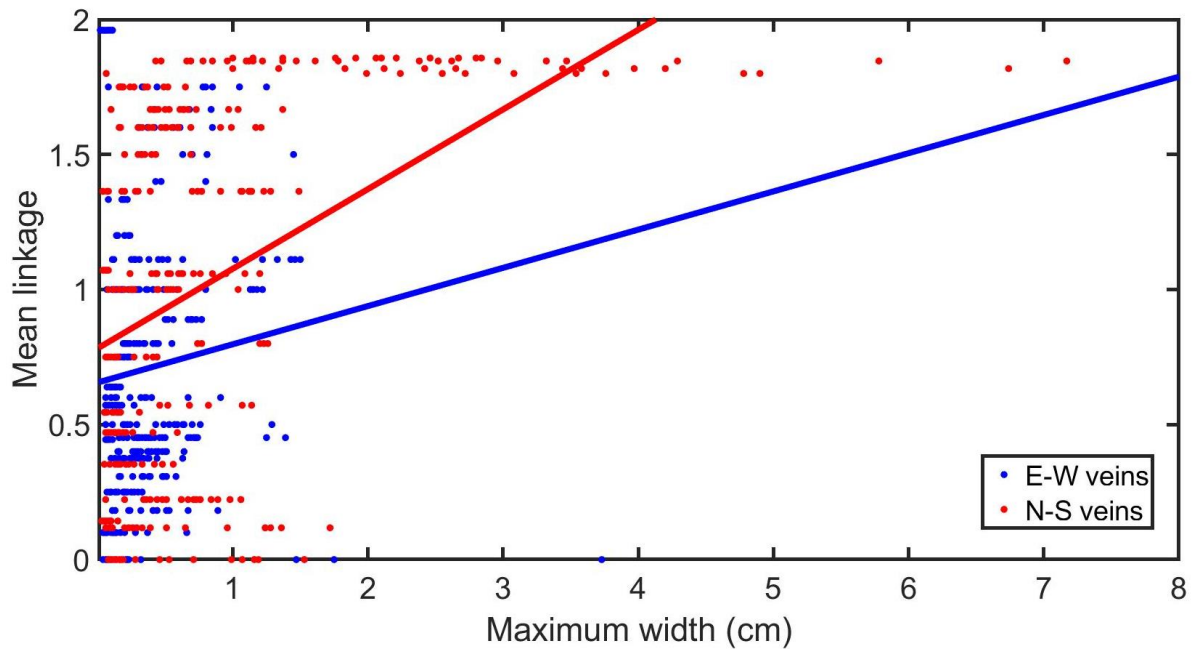


Figure 4.7 Graph of maximum widths plotted against mean linkages. The correlation coefficient is $\rho = 0.09$ for E-W veins, and $\rho = 0.47$ for N-S veins. The coefficient for N-S veins is surprising giving the poorly fitted regression line.

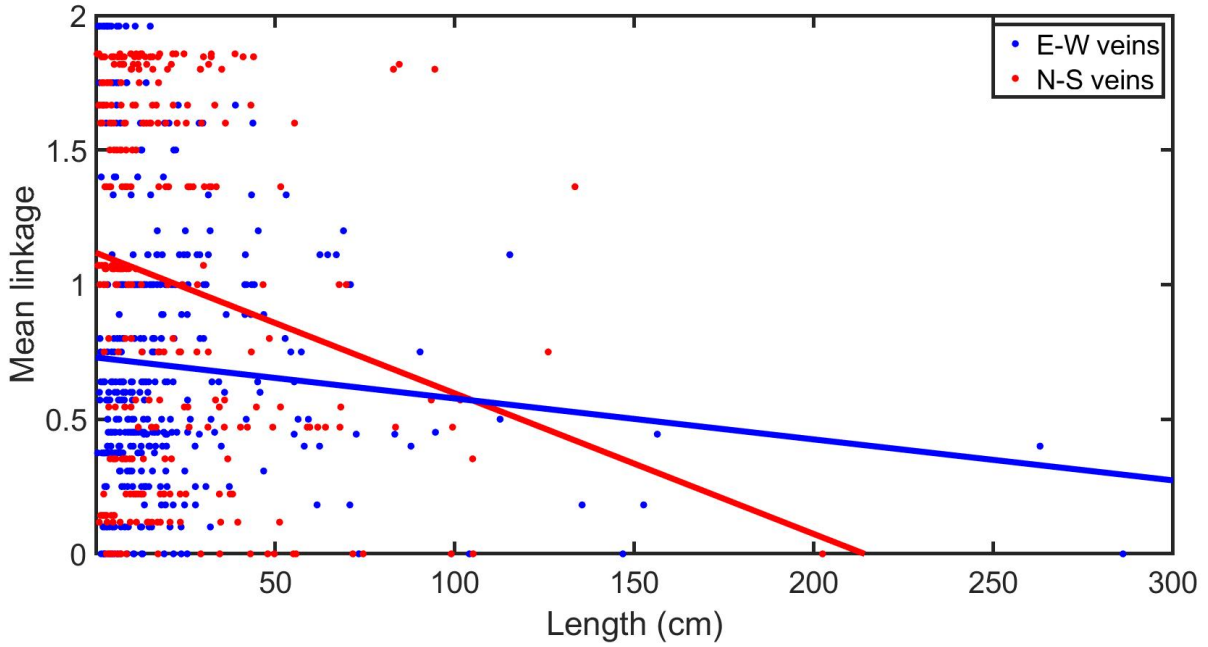


Figure 4.8 Linear regression analysis of the relationship between lengths and linkages, indicating no apparent correlation, reflected by the highly distributed scatter plot and the inability to display a regression line. The correlation coefficient is $\rho = -0.08$ for E-W veins and $\rho = -0.19$ for N-S veins.

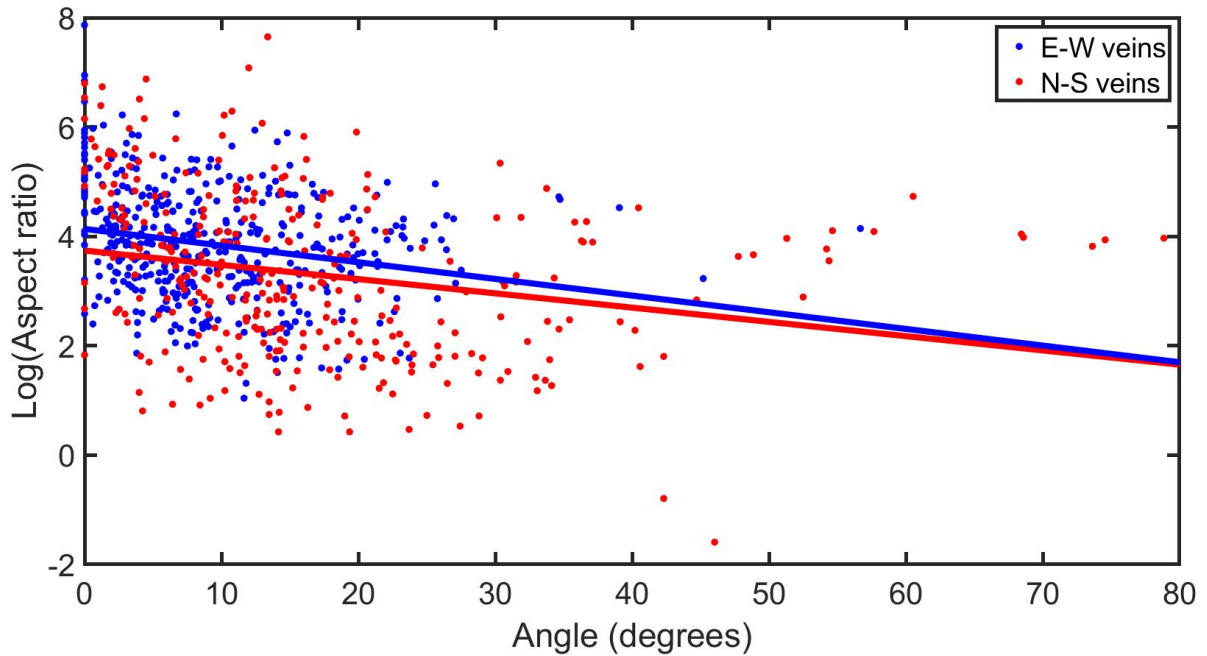


Figure 4.9 Scatter plot of angles and aspect ratios indicating a negative correlation for both orientations. The Correlation coefficients for both E-W and N-S veins are $\rho = -0.20$. The few vein segments that are measured above 45° are predominantly orientating N-S.

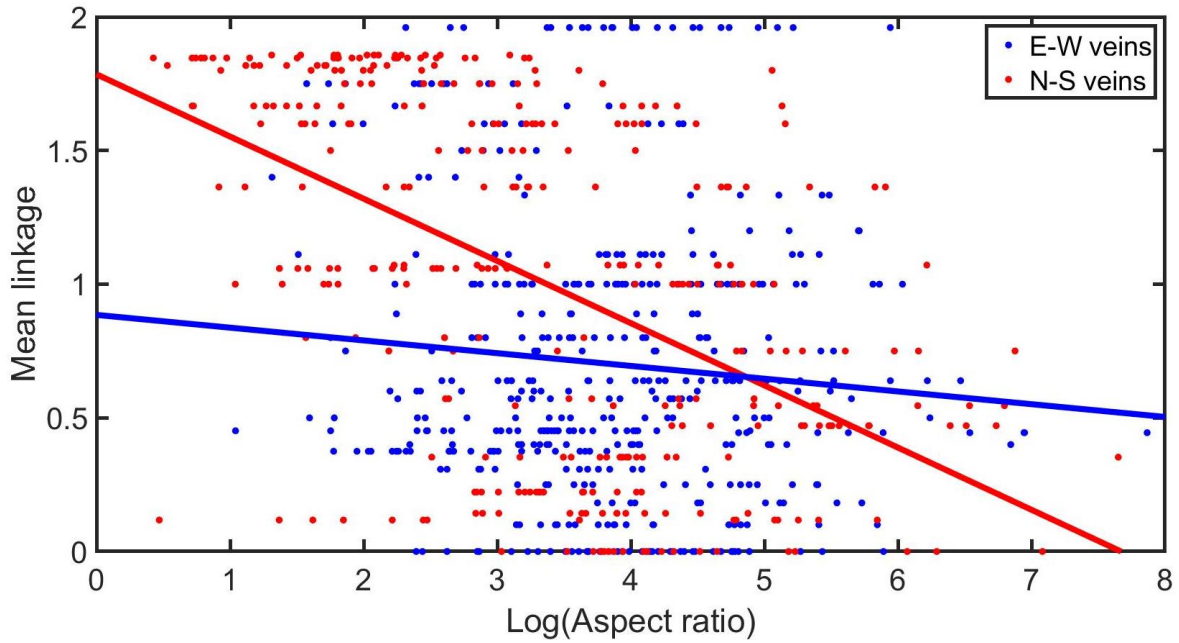


Figure 4.10 Graph showing the logarithm of aspect ratios plotted against the mean linkages. The E-W veins are showing a much weaker correlation than the N-S veins, reflected through the correlation coefficient of $\rho = -0.05$ and $\rho = -0.27$, respectively.

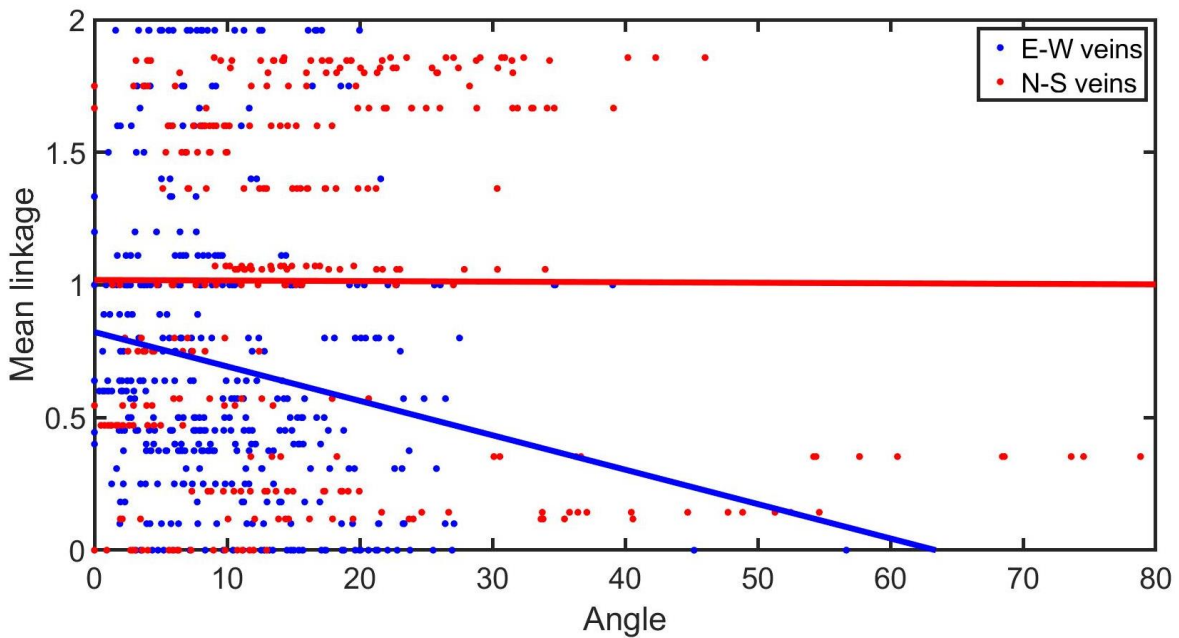


Figure 4.11 Angles and mean linkages shows no indication of correlation, as the method of least-square regression is not able to find a suitable fitting. The correlation coefficients for E-W veins and N-S veins are $\rho = -0.18$ and $\rho = -0.004$, respectively.

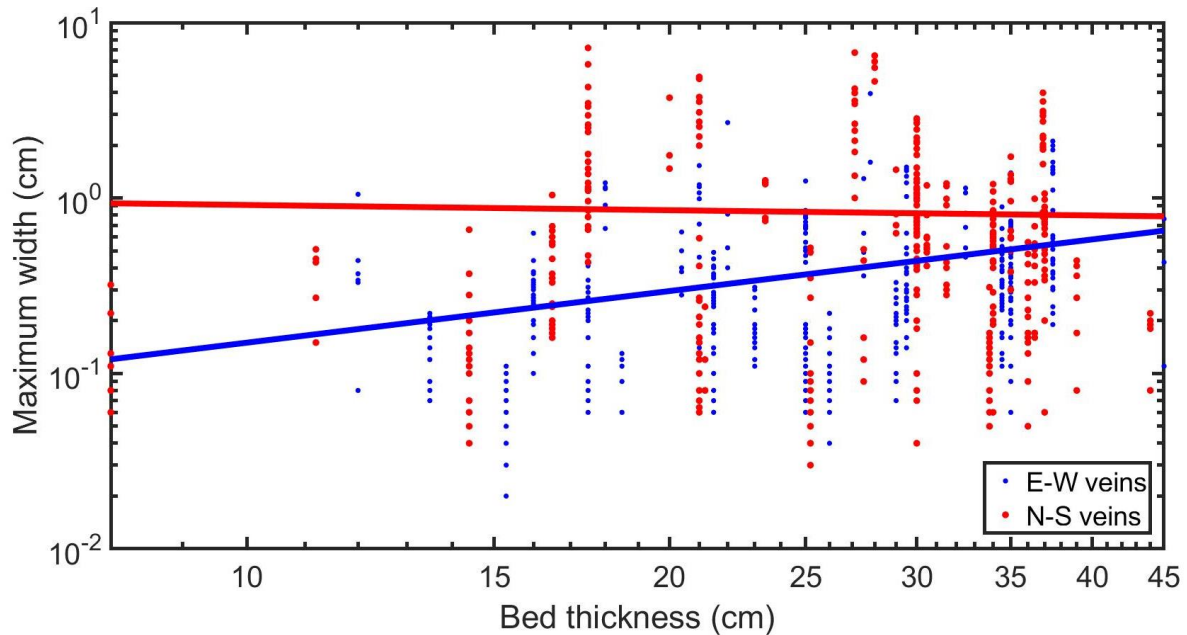


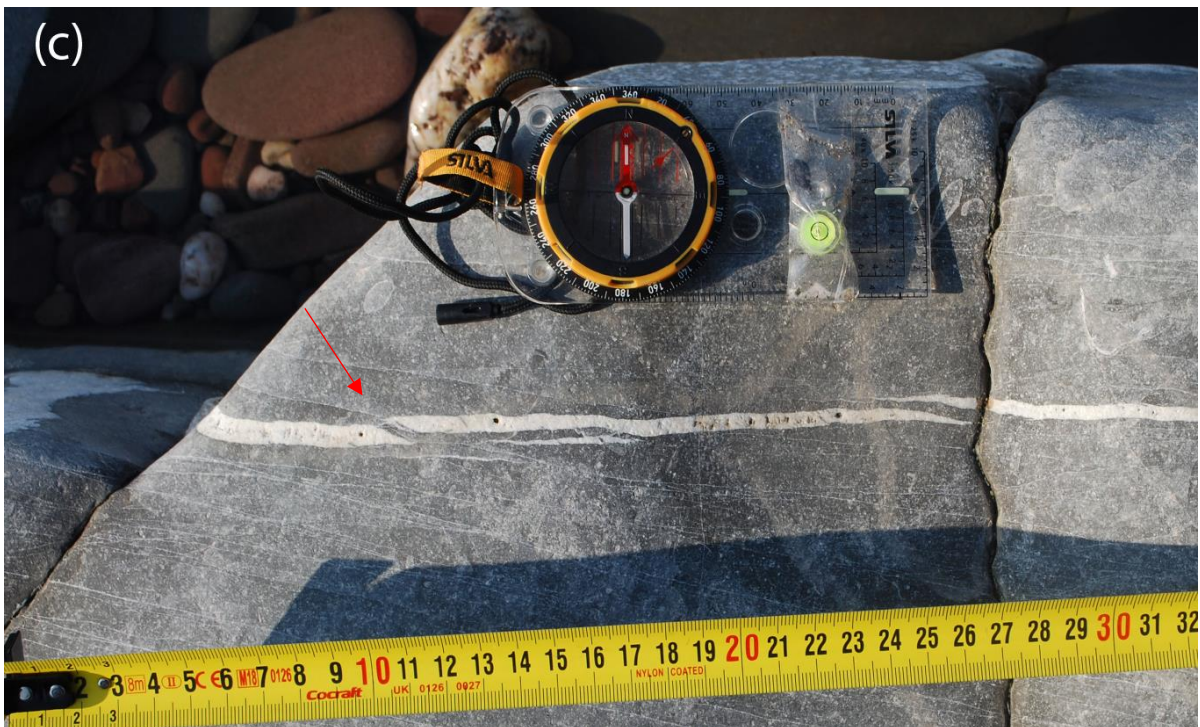
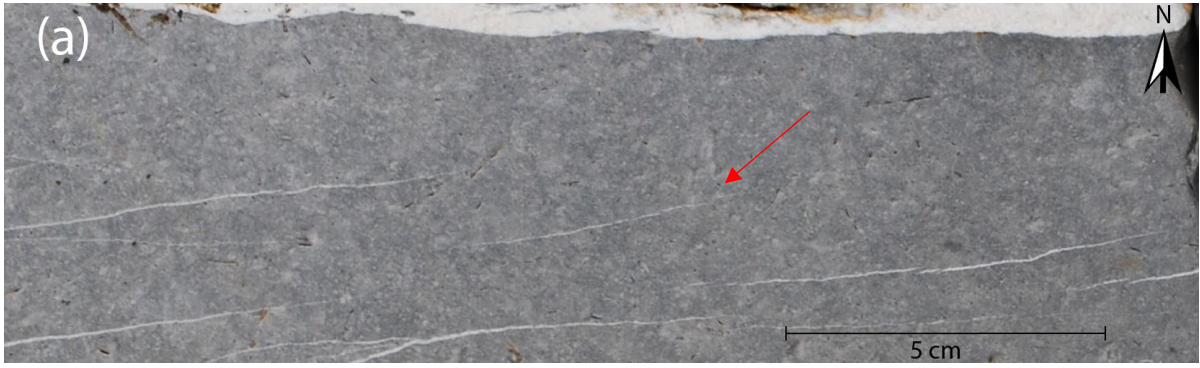
Figure 4.12 For E-W orientated veins the maximum widths show a moderate correlation coefficient of $\rho = 0.28$ with bed thickness. The trendline indicates that the maximum width increases with increasing bed thickness. For N-S orientated veins these two parameters had a coefficient of $\rho = -0.028$. Note that both axes are in logarithmic scale.

4.3 Ambiguities in the statistics

The least-squares regression used for estimating the relationship between the parameters in Section 4.2 is sensitive to outliers (Haenlein & Kaplan, 2004), meaning a few outliers would decrease the coefficient significantly. Outliers are defined as observations, which deviate markedly from the other members of the dataset (Niven & Deutsch, 2012). The data presented in Section 4.2 appears to not have many outliers, because of the high distribution (Table 4.1). Further, the method of regression has a high uncertainty for small datasets (Niven & Deutsch, 2012), which applies particularly for low correlations. Due to the very low correlations presented in Section 4.2 expanding the datasets should be considered.

4.4 Propagation, interaction and linkage

The observations of veins identified an interaction between segments before linkage. Veins that are distant to other segments show little to no alteration in their shape (Figure 4.13.a). Closer vein segments tend to adjust their shape to one another, often mirroring their tip geometry and bending their bridges (Figure 4.13.b). Some of these interacting segments show initiation of bridge failure (Figure 4.13.c). Others show broken bridges between two segments (Figure 4.13.d). Lastly, there are veins with very thin broken bridges, which is further interacting and initiating bridge failure (Figure 4.13.e). The arrays were also observed to often represent the tip of the damage zone of a fault or occur in the wall of a normal or strike-slip fault.



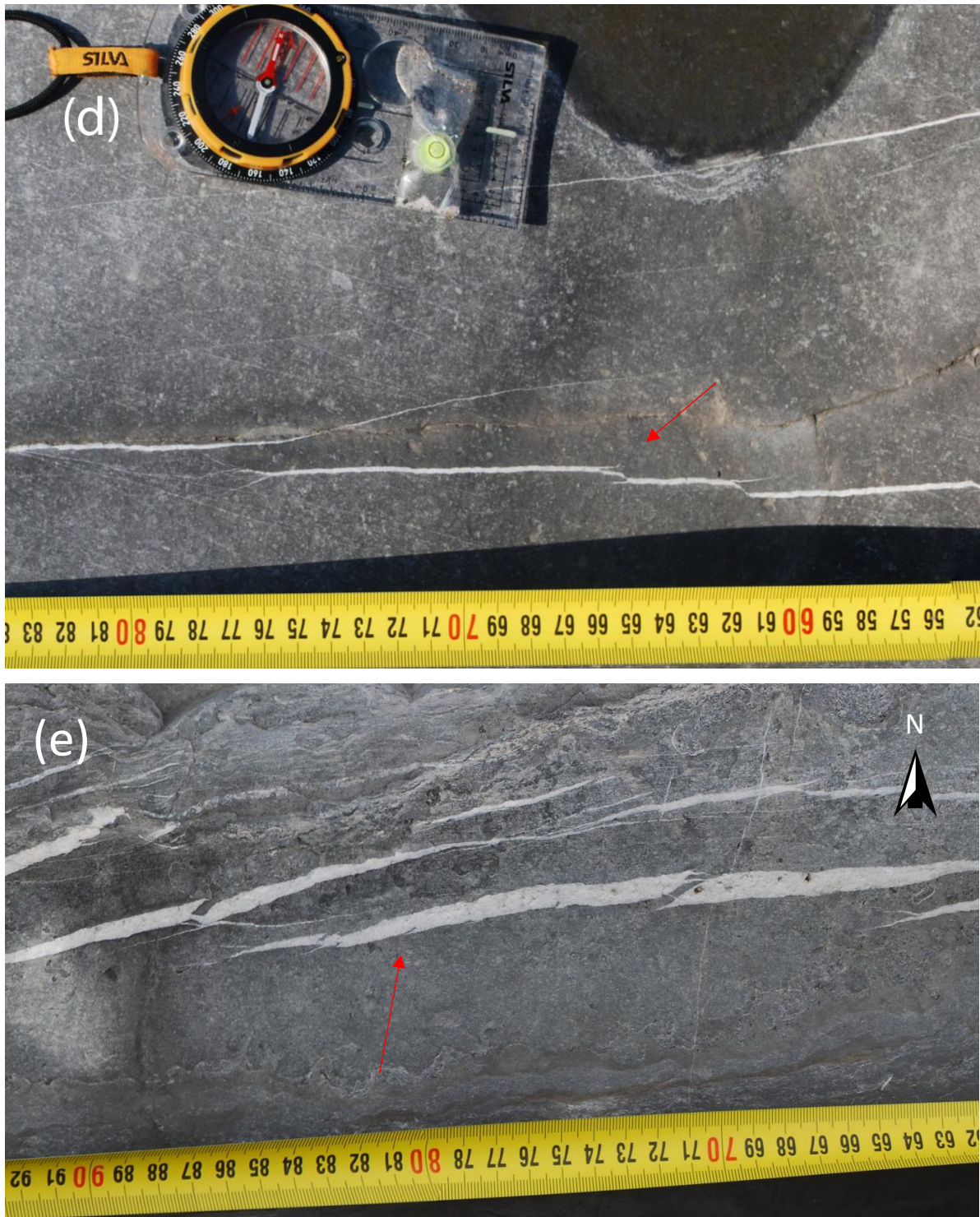


Figure 4.13 (a) Photograph of a vein segment which shows little to no interaction with adjacent veins. (b) Photograph of two vein segments interacting at the tips and transferring displacement through bending of bridges. The tips are shaped after each other creating a mirroring effect. (c) Two interacting tips showing an initiated bridge failure. (d) The bridge is breached, thus linking two segments together. (e) Photograph of a vein segment with thin broken bridges, the segment as a whole is further interacting and linking with an adjacent segment.

5 Interpretation

The results presented in Section 4.2 showed extensive scatter (Table 4.2). As a result, most relationships were not effective for discussing vein development. The weak correlation applied for length to width relationships as well, which is somewhat surprising considering Vermilye and Scholz (1995) stated that vein length expands proportionally to the aperture (see Section 2.2.2). Section 5.1 is therefore dedicated to explaining how propagation, interaction and linkage between segments are causing scatter in length to width plots. Then, Section 5.2 discusses how there are problems in the measurement methods.

5.1 The effects of vein propagation, interaction and linkage on data scatter

The maximum width increases with increasing length for both orientations of veins (Figure 4.6). The correlation is, however, weak (Table 4.2) which can partly be explained how they propagate, interact and link up. Peacock (1991) recognises three stages in the development of vein segments. Stage 1 includes isolated vein segments that do not interact with adjacent segments. These veins follow a constant aspect ratio, as illustrated by line 1 on Figure 5.1. Stage 2 is when the veins start to interact, causing decrease in the rate of length increase, although the dilation continues (line 2 on Figure 5.1). Stage 3 is when the vein connects, which makes the two segments share length, thereby increasing the length with a relatively fixed maximum width (line 3 on Figure 5.1). The stages then repeat itself creating a stepwise pattern similarly to faults (Cartwright et al., 1995). The stepwise pattern will therefore have a scattering effect on the length to width plot. Note that this growth path considers a single vein segment, whether or not it is composed of several linked segments, i.e. the linkage value = 0.

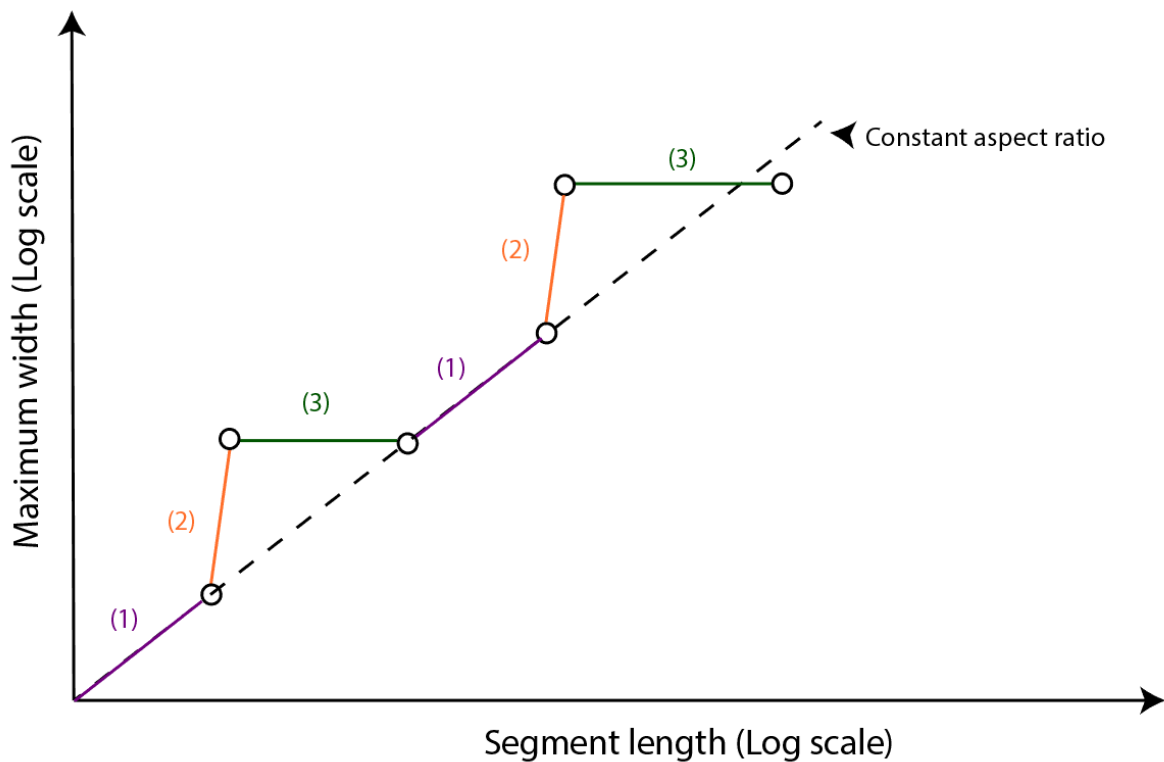


Figure 5.1 Illustration of the growth path for a vein segment. (1) Constant aspect ratio for isolated vein segments, where the length and width grow proportionally. (2) Interaction between two segments hinders propagation but the segment continues to increase in width. (3) The vein segments connect causing the segments to have shared length, thus increasing the length relatively to the width. For a similar model for faults, see Cartwright et al. (1995).

The three stages in the development of vein segments can be identified in the veins presented in Section 4.4. The vein in Figure 4.13.a represents stage 1 in the development of segments. A normalisation plot demonstrates that the veins do not overlap nor interact (Figure 5.2.a). The vein in Figure 4.13.b represents stage 2 where segments interact, and width is transferred by bending or rotating the bridge (Figure 5.2.b; Nicholson & Pollard, 1985). The vein in Figure 4.13.c represents a transition between stage 2 and 3. The bridge begins to be broken down by a fracture which links the segments (Figure 5.2.c). The vein in Figure 4.13.d represents stage 3 where the bridge is breached. The linkage point is identified by a width minimum in a normalisation plot (Figure 5.2.d). The vein in Figure 4.13.e reflects a repetition of the three stages of propagation, interaction and linkage. Here, however, the composite vein is further interacting and linking with an adjacent vein segment (Figure 5.2.e).

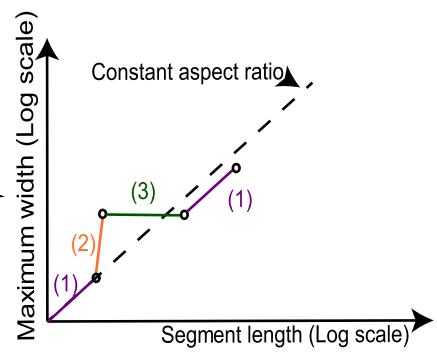
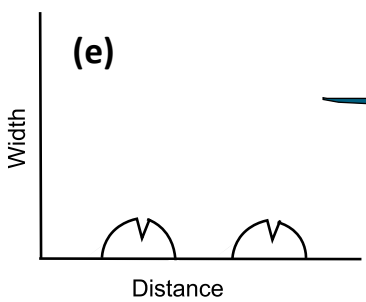
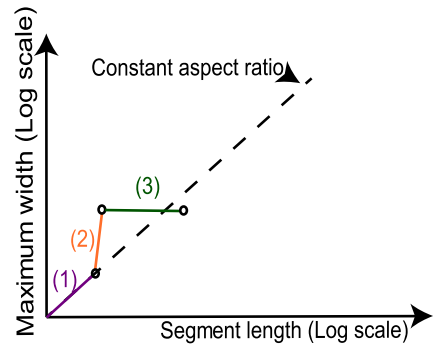
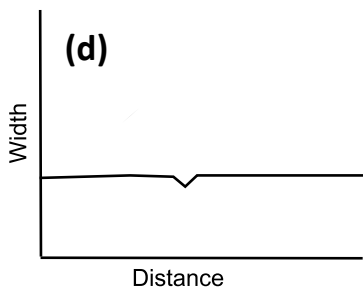
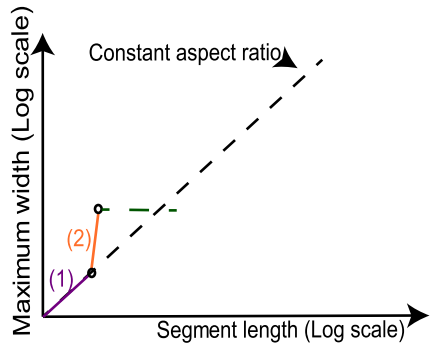
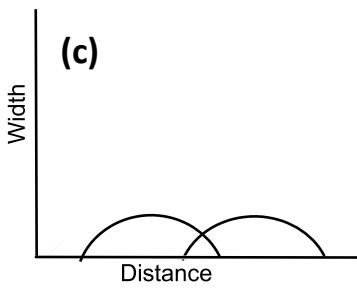
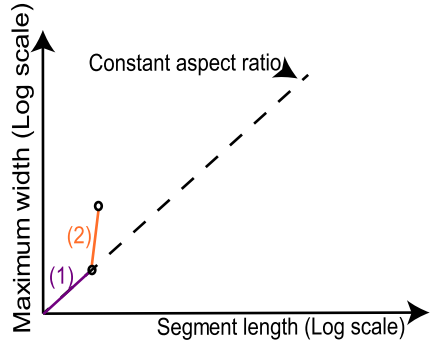
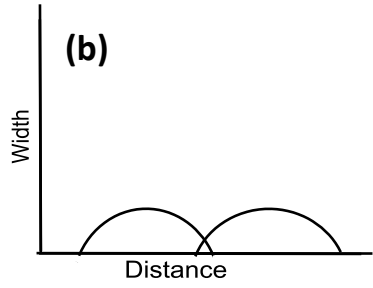
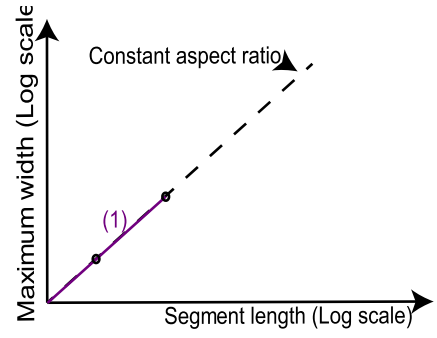
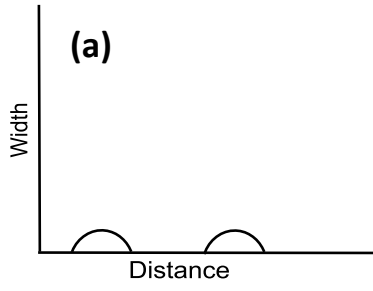


Figure 5.2 (a) In stage 1 the vein segment is not interacting with adjacent segments. (b) In stage 2 the vein segment is interacting, and the width is transferred by forming a bridge. (c) A transition stage between stage 2 and stage 3, where the bridge begins breach by initiate fractures. (d) In stage 3 the bridge is fully breached, and therefore the two segments are linked. The linkage area is identified by a small width minimum in a normalisation plot. (e) Here the stages are repeated, and the composite segment starts to interact and link with other adjacent segments.

The magnitude of the growth by linkage is controlled by the degree of overlap between the two linked segments. The composite vein formed from the previously unconnected segments will have a length that is the sum of the two older vein segments minus the length of the overlapping area (equation 5.1):

$$L = (\sum_{i=1}^n l_i) - (\sum_{i=1}^{n-1} a_i) \quad (5.1)$$

where L is the length of the composite segment, n is the number of segments originally, l is length of individual segments and a is the length of the overlapping area. This way the scattering effect is larger for vein segments with a short overlapping area. As mentioned in Section 3.1 Beach (1975) concluded angle to increase proportionally to the degree of overlap. Table 4.1 shows that E-W veins have a generally lower angle in comparison to N-S veins, which implies that the scattering effect of growth by linkage is larger for E-W veins. Table 4.2, however, shows that E-W veins have a higher linear correlation than N-S veins, which is because of pull-apart development. When veins develop into pull-aparts, the width increases relatively to the length because the veins develop into a fault with shear displacement. This decreases the aspect ratio and therefore causing deviation from the constant aspect ratio. The addition of shear displacement can partly explain why the veins have a greater mean width in the N-S dataset compared to the E-W dataset (Table 4.1).

5.2 Problems with the measurements

The repetitive cycle of propagation, interaction and linkage is forming a sense of self-similarity in the vein segments. The idea of self-similarity for faults was proposed by Tchalenko (1970), which means that the fracture is approximately similar to a part of itself. The self-similarity in veins generates a problem when defining segments. E.g. the vein in Figure 4.13.e it is arbitrary where one should delimit the segments. To illustrate this issue two different delimitations for one vein has been marked in Figure 5.3. Measuring the whole vein is equally convincing as measuring the vein as 5 segments. The effects of these two delimitations in a length to width plot shows either a cluster of shorter segments or one longer segment (Figure 5.4). The problem with defining segments also affects linkage plots, where it shows either several points with linkage = 2 or one with linkage = 1 (Figure 5.5).



Figure 5.3 Two different delimitations of the same vein. Green divides the vein into 5 segments, whereas red identifies the vein as one segment.

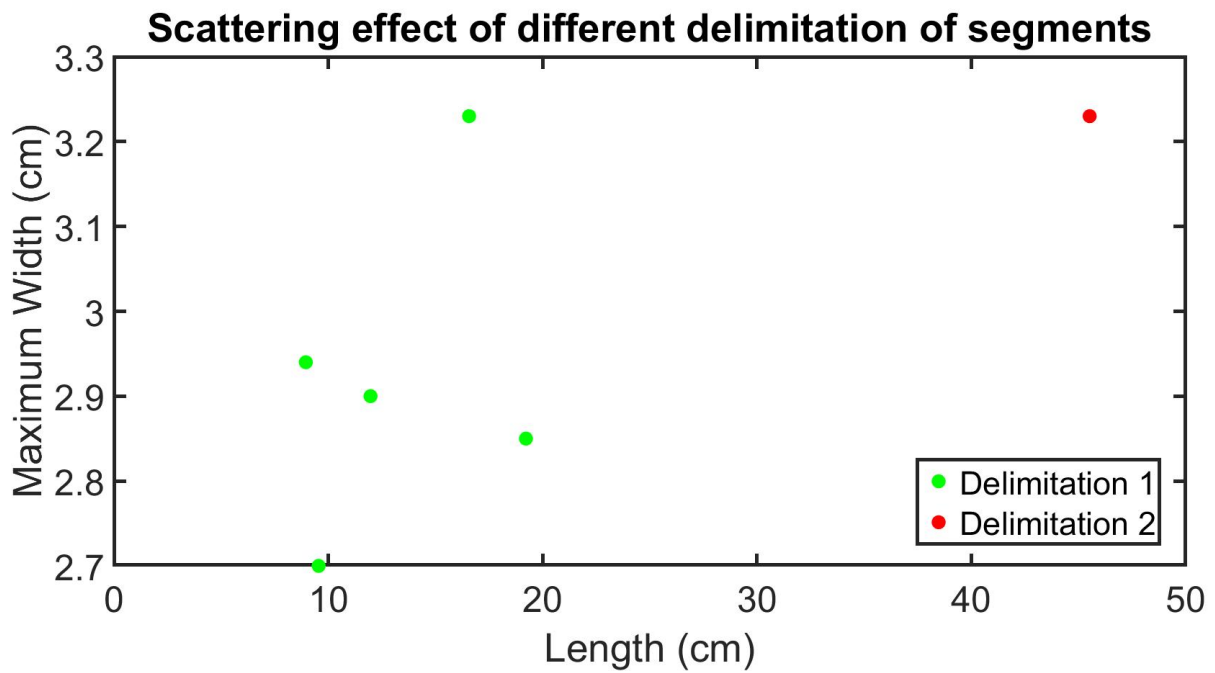


Figure 5.4 The graph is showing the plotted length and width measurements from the two delimitations in Figure 5.3. The vein shows either a cluster of shorter segments or one longer.

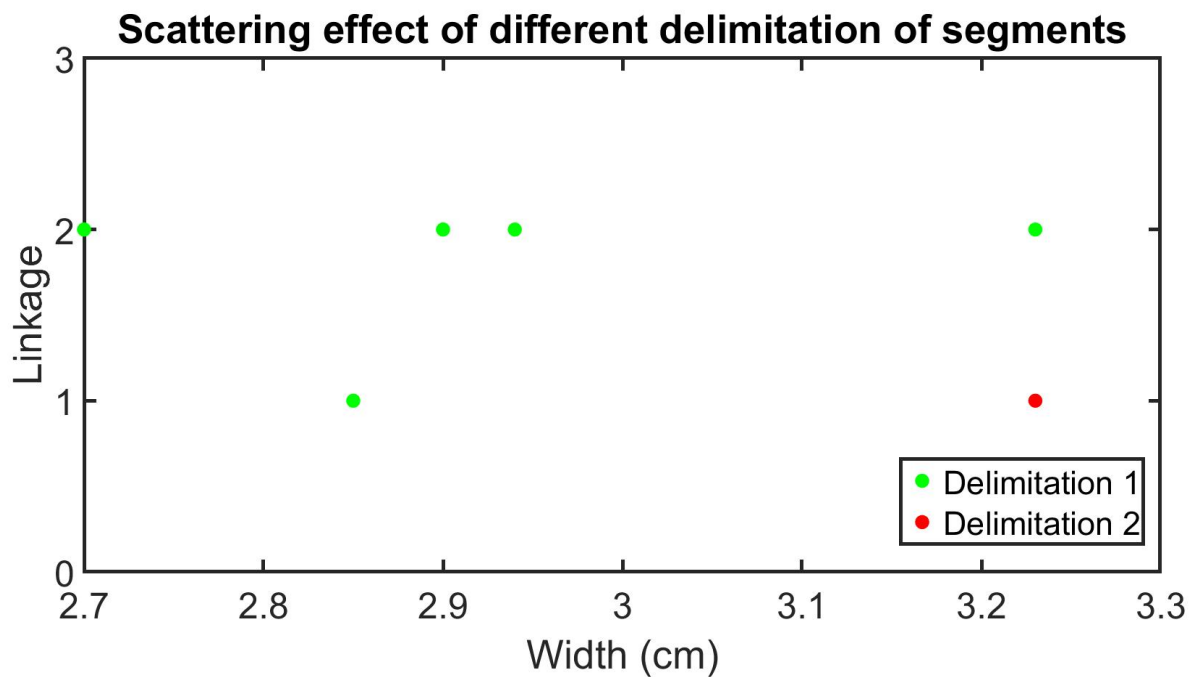


Figure 5.5 The graph is showing the plotted linkage and width measurements from the two delimitations in Figure 5.3. The vein shows either 5 segments with linkage = 2 or 1 segment with linkage = 1.

Peacock and Sanderson (1995) present a model to illustrate the different geometries for veins and pull-aparts, with varying amount of transpression/transtension. The model shows that lower segment angles ($\sim 0^\circ$) represent extensional displacement moderate angles ($\sim 45^\circ$) represent simple shear, while angles of $> 45^\circ$ indicate transpression. The E-W veins are commonly associated with normal faults, which is why their angles indicate extensional to transtensional displacements (Table 4.1). Vein arrays with an extensional displacement form at a low angle to the boundaries of the array (θ) (Figure 5.6.a). The N-S orientated veins are associated with strike-slip faults, and tend to show evidence of transtension or simple shear, there being a higher angle between the segments and the array boundary (Figure 5.6.b; Peacock & Sanderson, 1995). The E-W and N-S vein sets show different normalisation plots of segment angles (Figure 4.3), with the E-W orientated veins showing generally lower angles than the N-S orientated veins. There is, however, evidence of shear in some of the E-W veins. For example, Figure 5.7 shows an E-W orientated vein array with a sigmoidal shape. The sigmoidal shape is an indicator that the veins have been distorted by progressive simple shear deformation (Beach, 1975). The presence of simple shear in some of the E-W orientated vein arrays can explain some of the high angle arrays in the E-W dataset (Figure 4.3; Figure 4.9). Rotevatn and Peacock (2018) argue for strike-slip reactivation on some of the normal faults east of Lilstock, which overlaps with this thesis study area (see Figure 1.1). The strike-slip reactivation on some of the normal faults explains the evidence of simple shear in some of the E-W orientated vein arrays. It can therefore more be useful to separate the E-W veins in this area from the veins recorded west for Lilstock. It could also be beneficial to divide the dataset based on angle to the zone rather than orientation.

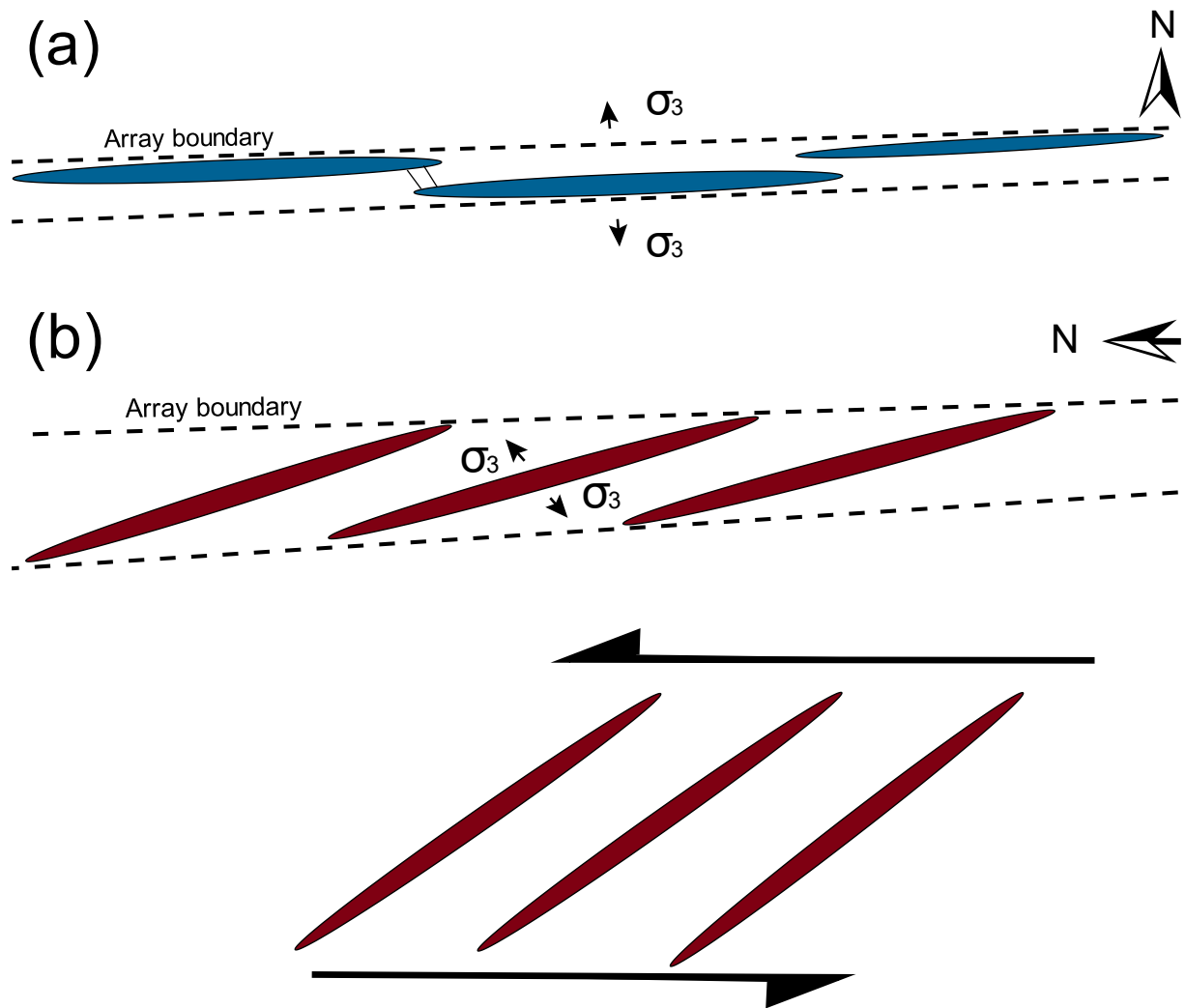


Figure 5.6 (a) Schematic illustration of a common E-W orientated array. The veins range from purely extensional to slightly transtensional, as indicated by the low angle between the veins and the boundaries to the array (Table 4.1). (b) Schematic illustration of two common N-S orientated veins arrays. The upper array is transtensional, whereas the lower formed in simple shear, as indicated by the angle of 45° between the veins and the boundaries of the array.



Figure 5.7 The sigmoidal shape of the vein segments is evidence for a simple shear component in E-W orientated arrays. The vein is recorded in the area east of Lilstock, see map in Figure 1.1.

6 Discussion

Section 6.1 discusses the definition of segments and how to manage the problems segmentation leads to. The section further discusses two methods for defining segments in vein arrays. Section 6.2 compares the progradation, interaction and linkage of veins with fault development, followed by how it is problematic for seismic interpretations.

6.1 What is a segment?

Segments can be constructed by linkage of smaller segments, thus creating self-similar geometries. A segment, however, cannot have an infinitely repeating self-similarity. It is, therefore, possible that the self-similarity of segments occurs to microscopic scales. Peacock et al. (2016) define a segment as “an individual fracture plane that is part of a set of subparallel fractures that forms a fracture zone” (Section 2.2.1). The definition, however, does not specify how to manage segmentation when measuring geometric values. To acquire better correlations between parameters, different approaches for defining segments should be discussed. The method practiced in this thesis is a topological approach, which defines the segments based on visible linkage points (Figure 6.1.a). As Section 5.1 demonstrated, segmentation occurs at millimetre and centimetre scales. The possibility of self-similarity occurring at smaller scales implies that the topological approach is significantly influenced by the resolution in the measurements. Observing a vein segment with a higher resolution can, therefore, reveal further segmentation. The method, however, has a clear distinction between linked and unlinked segments.

An alternative approach for defining segments can be through kinematic interactions. In this approach, the end points are set to the tips of a vein despite having topological linkage points within (Figure 6.1.b). Linkage is therefore assigned based on interaction with adjacent vein segments. Interaction is determined by an alteration in shape at the tip of a segment, and the development of a bridge (Figure 6.2). A vein segment interacting at both tips is, therefore, categorised as linkage = 2. A vein segment interacting at one tip is categorised as linkage = 1, and an isolated segment is categorised as linkage = 0 (Figure 6.2). Assigning linkage based on kinematics will not demonstrate a self-similar pattern, because there

cannot be interactions within an intact vein. The method, however, is ambiguous in terms of identifying interactions. It can be difficult to determine whether a shape alteration is caused by interaction or other processes. Additionally, a shape alteration can be slight therefore difficult to identify.

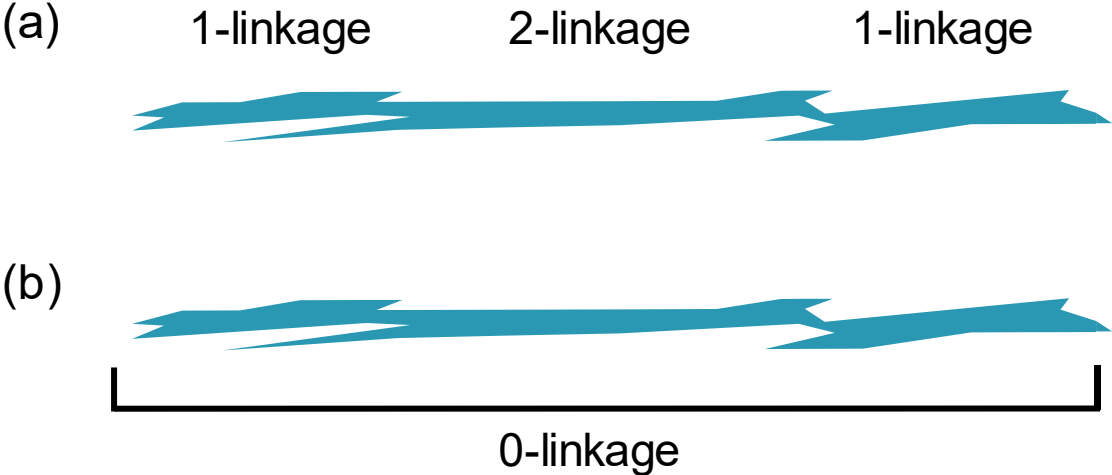


Figure 6.1 (a) In the topological approach, the segments are defined based on visible linkage point. The vein, therefore, consists of three segments with a linkage value of 1, 2 and 1. (b) In the kinematic approach the segments are defined by the tips of the vein. The linkage value is therefore 0.



Figure 6.2 The three vein segments have assigned linkage value based on their interaction with adjacent veins. The interaction is determined by a shape alteration of the segment tips, which develops a clear bridge. A vein segment with kinematic interaction at both tips is assigned linkage value 2, a vein segment with kinematic interaction at one tip is assigned linkage value 1, and an isolated vein segment is assigned linkage value 0. The vein is from the area between Lilstock and East Quantoxhead.

As for time being there seems to be no correct way to define vein segments. Both methods discussed here have extensive ambiguities and are therefore not satisfactory for relationship analysis. However, it is necessary to assess the issue with segmentation to find a suitable method.

6.2 Comparison with faults

Peacock and Sanderson (1991a) propose a four-stage model for fault propagation, interaction and linkage, similar to the model presented for veins in Section 5.1. Stage 1 occurs when there is no interaction with another fault segment, therefore there are no developed overstep between the fault segments (Figure 6.3a). Overstep is the area between two sub-parallel faults (Peacock et al., 2016). Stage 2 is when the displacement between two fault segments is transferred by rotation of the relay ramp (Figure 6.3.b). Stage 3 occurs when connecting faults develop across the relay ramp (Figure 6.3.c). In Stage 4 one connecting fault often becomes dominant, producing a fault-bend approximately parallel to

the displacement direction (Figure 6.3.d; Peacock & Sanderson, 1991a). The development of bridges appears to be comparable to the development of relay ramps, because of the way both transfer displacement by rotation (Peacock, 1991). Additionally, both bridges and relay ramps show a width/displacement minimum in a normalisation plot. Furthermore, veins and fault segments are both linked by failure of bridges/relay ramps. When the bridges/relay ramps are destroyed they are left as remnants in the composite vein/fault. Figure 4.13.e shows that the bridges are left as indentations in the composite vein, whereas relay ramps produce a fault-bend in the composite fault (Peacock & Sanderson, 1991a). As a result, the propagation, interaction and linkage of veins can be analogous to that of faults. The analogy between veins and faults makes it possible to study veins to understand faults better.

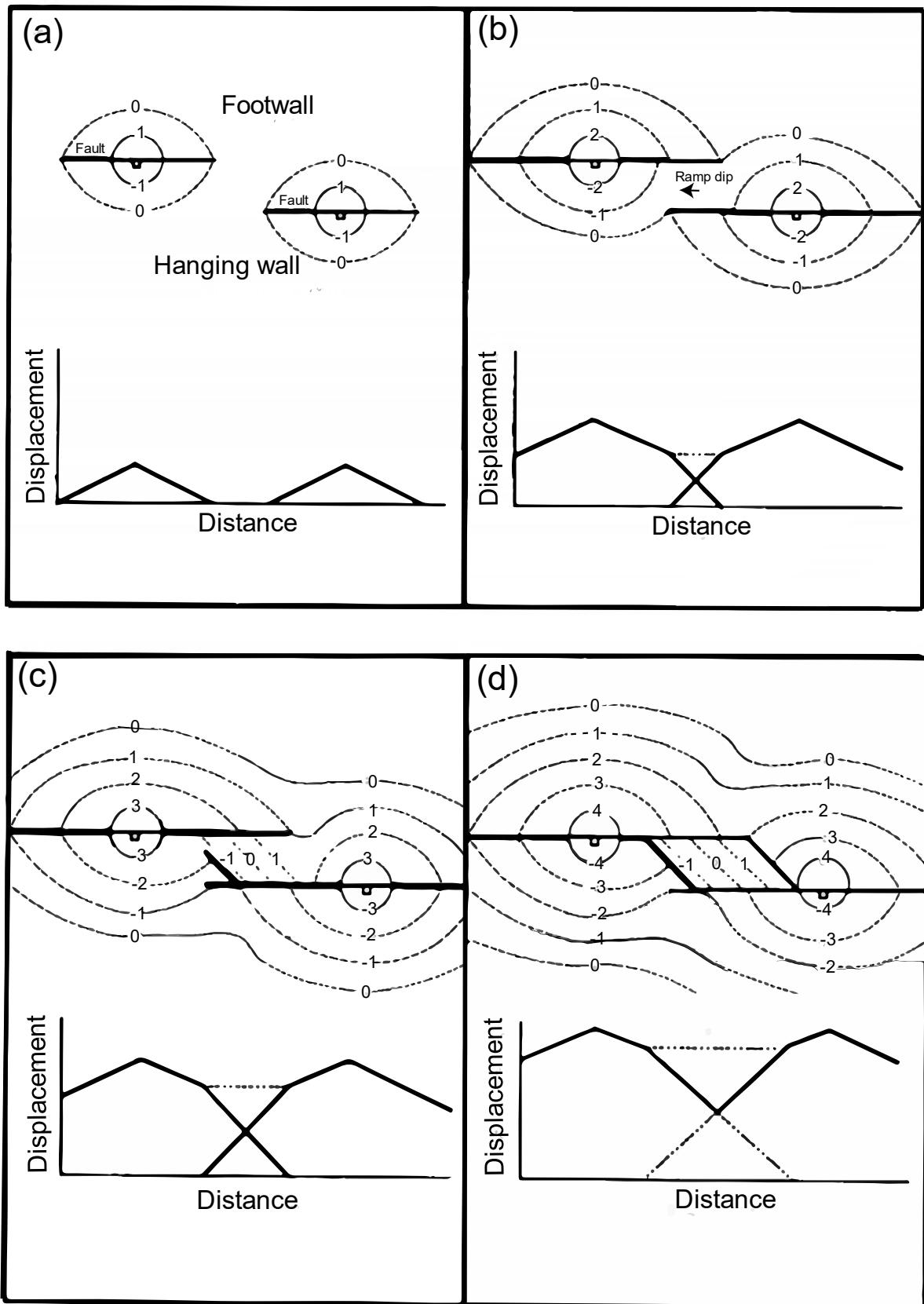


Figure 6.3 Schematic diagram of distance to displacement graphs and structural contour of a relay ramp development. The faults are dipping downwards in the figure and the contour lines are height above a datum level. (a) In stage 1 the fault segment is not interacting with adjacent segments. Thus, the distance to displacement plot is approximately linear. (b) In stage 2 the fault segment is

interacting, and displacement is transferred by rotation of the relay ramp. (c) Stage 3 where connecting fracture starts to link the overstepping segments. (d) In stage 4 the relay ramp is broken, forming a fault bend in map view. The illustration is modified from Peacock and Sanderson (1991b)

Cartwright et al. (1995) applies how fault propagate, interact and link to explain scatter in a length to displacement plot. Fault segments show a stepwise pattern in length to displacement development (Cartwright et al., 1995) in a similar way as veins (Figure 5.1), which supports the idea of faults being self-similar (Tchalenko, 1970). The self-similarity described for faults (e.g. Tchalenko, 1970) creates a problem when defining segments in seismic data. Pickering et al. (1997) concludes that fault segment length is underestimated on seismic data because the displacement at the tips is smaller than the resolution. Likewise, a displacement minimum can be overlooked because the decrease in displacement is less than the seismic resolution. The number of visible fault segments is therefore restricted by to the resolution of the seismic data.

7 Conclusions

The relationship between the geometrical parameters all show weak correlation (Table 4.2).

The weak correlations can be caused by three stages of vein segment development:

1) *Propagation*, where vein segment length and width increase at with an approximately constant ratio.

2) *Interaction*, where the vein segment interacts with one or more adjacent segments.

Propagation is hindered but aperture increases.

3) *Linkage*, where the interacting vein segments link, with the new composite vein segment having a greater length but the same maximum aperture as the original segments.

These three stages develop a stepwise pattern on a graph of segment length against maximum aperture. The process can repeat across a range of scales, creating self-similarity in vein segments.

A vein segment can be a composite of several smaller segments, which implies that the number of segments identified is determined by the resolution at which the system is observed. The way vein segments are defined therefore has an influence on the correlations between the measured parameters. A topological approach was taken in the analysis presented in this thesis, with vein segments characterised on whether the segment tips are physically linked to an adjacent vein segment. This may not be the best way to define segments. It is possible that using other methods to define vein segments will create better correlations between such parameters as length and maximum aperture.

The way faults propagate, interact and link is analogous to the veins, which explains their self-similarity. The self-similarity in faults causes problems with seismic interpretations, because the segmentation is controlled by the seismic resolution. It is therefore possible that using other methods to define fault segments will create better correlations between parameters such as length and maximum displacement.

8 References

- Beach, A. (1975). The geometry of en-echelon vein arrays. *Tectonophysics*, 28(4), 245-263.
doi:[https://doi.org/10.1016/0040-1951\(75\)90040-2](https://doi.org/10.1016/0040-1951(75)90040-2)
- Biddle, K. T., & Christie-Blick, N. (1985). Deformation and basin formation along strike-slip faults. *Society of economic mineralogists, Special publication 37*, 375-386.
- Bonnet, E., Bour, O., Odling, N. E., Davy, P., Main, I., Cowie, P., & Berkowitz, B. (2001). Scaling of fracture systems in geological media. *Reviews of Geophysics*, 39(3), 347-383.
doi:<https://doi.org/10.1029/1999rg000074>
- Bons, P. D., Elburg, M. A., & Gomez-Rivas, E. (2012). A review of the formation of tectonic veins and their microstructures. *Journal of Structural Geology*, 43, 33-62.
doi:<https://doi.org/10.1016/j.jsg.2012.07.005>.
- Cartwright, J., & Mansfield, C. (2001). Fault growth by linkage: Observations and implications from analogue models. *Journal of Structural Geology*, 23(5), 745-763.
doi:[https://doi.org/10.1016/S0191-8141\(00\)00134-6](https://doi.org/10.1016/S0191-8141(00)00134-6)
- Cartwright, J., Trudgill, B. D., & Mansfield, C. (1995). Fault growth by segment linkage: an explanation for scatter in maximum displacement and trace length data from the Canyonlands Grabens of SE Utah. *Journal of Structural Geology*, 17(9), 1319-1326.
doi:[https://doi.org/10.1016/0191-8141\(95\)00033-A](https://doi.org/10.1016/0191-8141(95)00033-A)
- Dart, C. J., McClay, K., & Hollings, P. N. (1995). 3D analysis of inverted extensional fault systems, southern Bristol Channel basin, UK. *Geological Society, London, Special Publications*, 88(1), 393-413. doi:<https://doi.org/10.1144/gsl.Sp.1995.088.01.21>
- Dawers, N. H., & Anders, M. H. (1995). Displacement-length scaling and fault linkage. *Journal of Structural Geology*, 17(5), 607-614. doi:[https://doi.org/10.1016/0191-8141\(94\)00091-D](https://doi.org/10.1016/0191-8141(94)00091-D)
- Engelder, T., & Peacock, D. C. P. (2001). Joint development normal to regional compression during flexural-flow folding: the Lilstock buttress anticline, Somerset, England. *Journal of Structural Geology*, 23(2-3), 259-277. doi:[https://doi.org/10.1016/S0191-8141\(00\)00095-X](https://doi.org/10.1016/S0191-8141(00)00095-X)
- Gibbs, A. D. (1984). Structural evolution of extensional basin margins. *Journal of the Geological Society*, 141(4), 609-620. doi:<https://doi.org/10.1144/gsjgs.141.4.0609>
- Haenlein, M., & Kaplan, A. M. (2004). A Beginner's Guide to Partial Least Squares Analysis. *Understanding Statistics*, 3(4), 283-287. doi:https://doi.org/10.1207/s15328031us0304_4

- Kemeny, J. (2005). Time-dependent drift degradation due to the progressive failure of rock bridges along discontinuities. *International journal of rock mechanics & mining sciences*, 42(1), 35-46.
- Lawrence, I. L. (1989). A Concordance Correlation Coefficient to Evaluate Reproducibility. *Biometrics*, 45(1), 255-268. doi:<https://doi.org/10.2307/2532051>
- McCoss, A. M. (1986). Simple constructions for deformation in transpression/transension zones. *Journal of Structural Geology*, 8(6), 715-718. doi:[https://doi.org/10.1016/0191-8141\(86\)90077-5](https://doi.org/10.1016/0191-8141(86)90077-5)
- Nicholson, R., & Pollard, D. D. (1985). Dilation and linkage of echelon cracks. *Journal of Structural Geology*, 7(5), 583-590. doi:[https://doi.org/10.1016/0191-8141\(85\)90030-6](https://doi.org/10.1016/0191-8141(85)90030-6)
- Niven, E. B., & Deutsch, C. V. (2012). Calculating a robust correlation coefficient and quantifying its uncertainty. *Computers & Geosciences*, 40, 1-9. doi:<https://doi.org/10.1016/j.cageo.2011.06.021>
- Olson, J. E. (2003). Sublinear scaling of fracture aperture versus length: An exception or the rule? *Journal of Geophysical Research*, 108(B9). doi:<https://doi.org/10.1029/2001JB000419>
- Olson, J. E., & Pollard, D. D. (1991). The initiation and growth of en échelon veins. *Journal of Structural Geology*, 13(5), 595-608. doi:[https://doi.org/10.1016/0191-8141\(91\)90046-L](https://doi.org/10.1016/0191-8141(91)90046-L)
- Peacock, D. C. P. (1991). A comparison between the displacement geometries of veins and normal faults at Kilve, Somerset. *Proceedings of the Ussher Society*, 7, 363-367.
- Peacock, D. C. P. (2004). Differences between veins and joints using the example of the Jurassic limestones of Somerset. *Geological Society, London, Special Publications*, 231(1), 209-221. doi:<https://doi.org/10.1144/gsl.Sp.2004.231.01.12>
- Peacock, D. C. P., Nixon, C. W., Rotevatn, A., Sanderson, D. J., & Zuluaga, L. F. (2016). Glossary of fault and other fracture networks. *Journal of Structural Geology*, 92, 12-29. doi:<https://doi.org/10.1016/j.jsg.2016.09.008>
- Peacock, D. C. P., Nixon, C. W., Rotevatn, A., Sanderson, D. J., & Zuluaga, L. F. (2017). Interacting faults. *Journal of Structural Geology*, 97, 1-22. doi:<https://doi.org/10.1016/j.jsg.2017.02.008>
- Peacock, D. C. P., & Sanderson, D. J. (1991a). Displacements, segment linkage and relay ramps in normal fault zones. *Journal of Structural Geology*, 13(6), 721-733. doi:[https://doi.org/10.1016/0191-8141\(91\)90033-F](https://doi.org/10.1016/0191-8141(91)90033-F)
- Peacock, D. C. P., & Sanderson, D. J. (1991b). Geometry and development of relay ramps in normal fault systems. *AAPG Bulletin*, 78(2), 147-165.

- Peacock, D. C. P., & Sanderson, D. J. (1995). Pull-aparts, shear fractures and pressure solution. *Tectonophysics*, 241(1-2), 1-13. doi:[https://doi.org/10.1016/0040-1951\(94\)00184-B](https://doi.org/10.1016/0040-1951(94)00184-B).
- Peacock, D. C. P., & Sanderson, D. J. (1999). Deformation history and basin-controlling faults in the Mesozoic sedimentary rocks of the Somerset coast. *Proceedings of the Geologists' Association*, 110(1), 41-52. doi:[https://doi.org/10.1016/S0016-7878\(99\)80005-4](https://doi.org/10.1016/S0016-7878(99)80005-4)
- Pickering, G., Peacock, D. C. P., Sanderson, D. J., & Bull, J. M. (1997). Modeling Tip Zones to Predict the Throw and Length Characteristics of Faults. *AAPG Bulletin*, January. doi:<https://doi.org/10.1306/522B4299-1727-11D7-8645000102C1865D>
- Pollard, D. D., & Aydin, A. (1988). Progress in understanding jointing over the past century. *Geological Society of America Bulletin*, 100, 1181-1204.
- Pollard, D. D., Segall, P., & Delaney, P. T. (1982). Formation and interpretation of dilatant echelon cracks. *GSA Bulletin*, 93(12), 1291-1303. doi:[https://doi.org/10.1130/0016-7606\(1982\)93](https://doi.org/10.1130/0016-7606(1982)93)
- Procter, A., & Sanderson, D. J. (2018). Spatial and layer-controlled variability in fracture networks. *Journal of Structural Geology*, 108. doi:<https://doi.org/10.1016/j.jsg.2017.07.008>
- Rawnsley, K. D., Peacock, D. C. P., Rives, T., & Petit, J.-P. (1998). Joints in the Mesozoic sediments around the Bristol Channel Basin. *Journal of Structural Geology*, 20(12), 1641-1661. doi:[https://doi.org/10.1016/S0191-8141\(98\)00070-4](https://doi.org/10.1016/S0191-8141(98)00070-4)
- Rotevatn, A., & Peacock, D. C. P. (2018). Strike-slip reactivation of segmented normal faults: Implications for basin structure and fluid flow. *Basin Research*, 30(6), 1264-1279. doi:<https://doi.org/10.1111/bre.12303>
- Sanderson, D. J., & Peacock, D. C. P. (2019). Measurement of geometry and linkage in vein arrays. *Journal of Structural Geology*, 118, 104-113. doi:<https://doi.org/10.1016/j.jsg.2018.10.001>
- Schofield, N., Heaton, L., Holford, S. P., Archer, S. G., Jackson, C. A.-L., & Jolley, D. W. J. (2012). Seismic imaging of 'broken bridges': linking seismic to outcrop-scale investigations of intrusive magma lobes. *Journal of the Geological Society*, 169(4), 421-426.
- Scholz, C. H., Anders, M. H., & Dawers, N. H. (1993). Growth of normal faults: Displacement-length scaling. *Geology*, 21(12), 1107-1110.
- Sheppard, T. H., Houghton, R. D., & Swan, A. R. H. (2006). Bedding and pseudo-bedding in the Early Jurassic of Glamorgan: deposition and diagenesis of the Blue Lias in South Wales. *Proceedings of the Geologists' Association*, 117(3), 249-264. doi:[https://doi.org/10.1016/S0016-7878\(06\)80033-7](https://doi.org/10.1016/S0016-7878(06)80033-7)

- Tchalenko, J. S. (1970). Similarities between shear zones of different magnitudes. *GSA Bulletin*, 81(6), 1625-1640. doi:[https://doi.org/10.1130/0016-7606\(1970\)81\[1625:Sbszod\]2.0.Co;2](https://doi.org/10.1130/0016-7606(1970)81[1625:Sbszod]2.0.Co;2)
- Van Hoorn, B. (1987). The south Celtic Sea/Bristol Channel Basin: origin, deformation and inversion history. *Tectonophysics*, 137(1-4), 309-334. doi:[https://doi.org/10.1016/0040-1951\(87\)90325-8](https://doi.org/10.1016/0040-1951(87)90325-8)
- Vermilye, J. M., & Scholz, C. H. (1995). Relation between vein length and aperture. *Journal of Structural Geology*, 17(3), 423-434. doi:[https://doi.org/10.1016/0191-8141\(94\)00058-8](https://doi.org/10.1016/0191-8141(94)00058-8)
- Walsh, J. J., & Watterson, J. (1988). Analysis of the relationship between displacements and dimensions of faults. *Journal of Structural Geology*, 10(3), 239-247. doi:[https://doi.org/10.1016/0191-8141\(88\)90057-0](https://doi.org/10.1016/0191-8141(88)90057-0)